3696–3721 *Nucleic Acids Research, 2023, Vol. 51, No. 8* *Published online 2 March 2023*
https://doi.org/10.1093/nar/gkad099

Differential requirements for Gcn5 and NuA4 HAT activities in the starvation-induced versus basal transcriptomes

Qiaoyun Zheng, Hongfang Qiu, Hongen Zhang and Alan G. Hinnebusch*

Division of Molecular and Cellular Biology, *Eunice Kennedy Shriver* National Institute of Child Health and Human Development, National Institutes of Health, Bethesda, MD 20892, USA

Received July 01, 2022; Revised February 01, 2023; Editorial Decision February 02, 2023; Accepted February 27, 2023

ABSTRACT

The histone acetyltransferase (HAT) subunit of coactivator complex SAGA, Gcn5, stimulates eviction of promoter nucleosomes at certain highly expressed yeast genes, including those activated by transcription factor Gcn4 in amino acid-deprived cells; however, the importance of other HAT complexes in this process was poorly understood. Analyzing mutations that disrupt the integrity or activity of HAT complexes NuA4 or NuA3, or HAT Rtt109, revealed that only NuA4 acts *on par* with Gcn5, and functions additively, in evicting and repositioning promoter nucleosomes and stimulating transcription of starvation-induced genes. NuA4 is generally more important than Gcn5, however, in promoter nucleosome eviction, TBP recruitment, and transcription at most other genes expressed constitutively. NuA4 also predominates over Gcn5 in stimulating TBP recruitment and transcription of genes categorized as principally dependent on the cofactor TFIID versus SAGA, except for the most highly expressed subset including ribosomal protein genes, where Gcn5 contributes strongly to PIC assembly and transcription. Both SAGA and NuA4 are recruited to promoter regions of starvation-induced genes in a manner that might be feedback controlled by their HAT activities. Our findings reveal an intricate interplay between these two HATs in nucleosome eviction, PIC assembly, and transcription that differs between the starvation-induced and basal transcriptomes.

INTRODUCTION

In the yeast *Saccharomyces cerevisiae,* most genes transcribed by RNA Polymerase II (Pol II) contain a nucleosome-depleted region (NDR) of ∼120 bp situated upstream of the coding sequences (CDS) flanked by highly positioned '–1' and '+1' nucleosomes, with the transcription start site (TSS) frequently located within the +1 nucleosome (henceforth +1_Nuc). Given its proximity to the TSS and adjacent upstream promoter elements, the +1_Nuc can interfere with formation of the preinitiation complex (PIC) and initiation of transcription. Accordingly, the +1_Nuc is frequently evicted (1,2) (3) or shifted in the 3' direction (4,5) (6) in the course of promoter activation. The yeast ATP-dependent chromatin remodeling complexes SWI/SNF and RSC, capable of sliding or evicting nucleosomes *in vitro*, serve to eliminate nucleosomes from NDRs, and also to reposition the +1 and –1 nucleosomes to maintain proper NDR widths. While RSC is important for establishing proper NDR widths at the majority of yeast genes (7–9) (10,11), SWI/SNF partners with RSC in performing this function, and also stimulating transcription, at the subset of most highly expressed genes, including those activated by the starvation-induced transcription factor Gcn4 (3,6).

The Gcn4 transcriptome provides an ideal subject for probing the *in vivo* requirements for chromatin remodelers and other coactivators in remodeling promoter nucleosomes and activating transcription initiation, as it comprises several hundred genes that are rapidly induced by Gcn4 on limitation for an amino acid, which can be achieved with the inhibitor of isoleucine and valine biosynthesis sulfometuron methyl (SM). Indeed, we showed recently that the chromatin remodeler Ino80 complex is required in addition to SWI/SNF and RSC for robust nucleosome eviction and transcriptional activation of many of the genes induced in SM-treated cells. Comparing the effects of deletion or depletion of the catalytic subunits of these remodelers revealed extensive interplay among the three remodelers in which certain induced genes require all three complexes, whereas others require only one or two of them in otherwise WT cells for efficient promoter nucleosome eviction (12). Furthermore, an increased requirement for SWI/SNF or RSC was revealed when one remodeler was inactivated or depleted in mutant cells lacking the other. We made similar findings when SWI/SNF was eliminated in cells containing or lacking Gcn5, the histone (HAT) subunit

*To whom correspondence should be addressed. Tel: +1 301 496 4480; Email: ahinnebusch@nih.gov

of the SAGA coactivator complex (3), indicating partial redundancy in the functions of these two coactivators with distinct biochemical functions (3). Functional interplay between Gcn5 and SWI/SNF, and of SWI/SNF with RSC, in promoter nucleosome eviction and transcription was also evident at constitutively expressed genes with the highest rates of transcription (3) (6). Thus, the SM-induced cohort of genes is a useful model for uncovering general principles of coactivator cooperation that apply to many other well-expressed genes in yeast.

It is generally considered that histone acetylation enhances promoter nucleosome remodeling by weakening electrostatic attraction between positively charged lysine residues in the histones and the phosphodiester backbone of DNA; or by facilitating recruitment of other coactivators containing moieties that interact with acetylated lysines, such as the bromodomain. Having observed previously that elimination of Gcn5 did not fully impair nucleosome eviction at many SM-induced genes, we wondered whether Gcn5 cooperates with other HATs in this process, similar to the functional cooperation we identified for different chromatin remodelers. In particular, we wished to examine the role of HAT complex NuA4, whose catalytic subunit (Esa1) is essential in yeast. Whereas Gcn5 acetylates H3 and H2B, Esa1 is responsible for most H4 and H2A acetylation in yeast (13); and we showed that NuA4, like SAGA, is recruited to the promoters of the Gcn4 target genes *ARG1* and *ARG4* in a manner strongly enhanced by SM-induction of Gcn4 (14). Accordingly, we set out here to determine the effects of disrupting the NuA4 complex by eliminating its nonessential scaffold subunit Eaf1 on promoter nucleosome eviction and transcriptional activation at both SM-induced and constitutively expressed genes. We showed previously that Eaf1 is required for recruitment of other NuA4 subunits to the *ARG1* and *ARG4* promoters, and for association of Esa1 with the Tra1 subunit (14)—a likely direct target of the Gcn4 activation domain (15) shared between NuA4 and SAGA. We also wished to determine whether depleting Eaf1 confers defects in nucleosome eviction or transcription in cells lacking Gcn5 to evaluate whether NuA4 and Gcn5 make independent, additive contributions to these processes at particular genes *in vivo*.

While this work was underway, Bruzzone *et al.* reported that depleting Gcn5, Esa1, or Tra1 (to affect both SAGA and NuA4 simultaneously) from the nucleus using 'anchor-away' technology broadly reduced H3 or H4 acetylation at promoters in a manner correlated with reductions in Pol II occupancy of the downstream CDSs; but surprisingly, did not confer altered occupancies or positions of promoter nucleosomes (16). This finding could indicate that histone acetylation is required principally for coactivator recruitment versus nucleosome remodeling. However, those results for Gcn5 differed from our previous findings on deletion of *GCN5,* which conferred widespread increases in promoter H3 occupancies in SM-treated cells (3). This discrepancy might reflect incomplete nuclear depletion of Gcn5 by anchor away, or a greater requirement for Gcn5 in Ile/Val-starved cells compared to the growth conditions employed by Bruzzone *et al*. Accordingly, we have analyzed mutant cells completely lacking Eaf1 and thus disrupted for NuA4, lacking Gcn5, or both lacking Gcn5 and depleted of nuclear Eaf1 by anchor-away, in both SM-treated and untreated cells. Our results indicate that deletion of either *GCN5* or *EAF1* impairs eviction of promoter nucleosomes at many of the ∼200 genes highly induced by SM, and at a large fraction of genes expressed constitutively in SM-treated cells. Whereas *gcn5Δ* and *eaf1Δ* confer comparable increases in promoter nucleosomes at the SM-induced genes, *eaf1Δ* confers a relatively greater defect at constitutively expressed genes. We also observe a broader effect on PIC assembly, monitored by TBP recruitment, and transcription on disrupting NuA4 versus eliminating Gcn5, whereas Gcn5 acts *on par* with NuA4 at both SM-induced genes and the highly transcribed subset of constitutively expressed ribosomal protein (RP) genes. Our findings provide strong evidence that promoter nucleosome eviction is a key function for both Gcn5 and NuA4 in promoting transcription throughout the yeast genome and reveal differential requirements for these two HATs in nucleosome eviction, PIC assembly, and transcription between starvation-induced and the majority of constitutively expressed genes. Comparing these findings to our previous analysis of mutations affecting the SWI/SNF and RSC complexes further reveals a high degree of cooperation between these two chromatin remodelers and the HATs Gcn5 and NuA4.

MATERIALS AND METHODS

Yeast strains and plasmids

All yeast strains employed are listed in Supplementary Table S2. WT strain BY4741 and *kanMX4*-marked deletion derivatives were described previously (17) and purchased from Research Genetics, and all deletions in these strains were verified by PCR analysis of genomic DNA. The *gcn5Δ::hphMX4* allele was introduced into wild type strain HQY1695, engineered previously for anchor-away experiments (12), by gene replacement with a *gcn5Δ::hphMX4* fragment PCR-amplified from plasmid pFA6-hphMX4 (18) (19) to produce strain QZ15, which was verified by PCR analysis of the *GCN5* locus in QZ15. The same method was used to introduce *eaf1Δ::hphMX4* into HQY1695 to generate QZ16, and to introduce *gcn5Δ::hphMX4* into H4268 to produce QZ21, which were verified by PCR analysis of the *EAF1* or *GCN5* locus in the resulting strains. Anchor-away alleles of *GCN5* or *EAF1* were introduced into HQY1695 by C-terminal tagging with the coding sequences of FRB, producing QZ17and QZ18, using PCR-based methodology (18) and plasmid pHQ2142 as template, encoding the FRB tag and *natMX4* selective marker as described below. QZ19 was generated from QZ15, and QZ20 was produced from QZ16, by the same strategies. *SPT7-MYC$_{13}$::HIS3* or *SRB6-MYC$_{13}$::HIS3* alleles were introduced into strain H4311 by PCR-amplification of DNA containing the corresponding alleles from genomic DNA of yeast strains H3587 or H3617, respectively, and used to transform H4311 to a His$^+$ phenotype. The resulting gene replacements in strains QZ25 and QZ24 were verified by PCR analysis.

All plasmids employed in this work are listed in Supplementary Table S4, and all primers utilized in plasmid or strain constructions are given in Supplementary Table S3. Plasmids pQZ2-pQZ5 were produced by isolating DNA fragments containing the appropriate WT genes by PCR

amplification from WT yeast genomic DNA and inserted into YCplac33. The inserted fragments were sequenced in their entirety and shown to complement the corresponding yeast mutants. pQZ2 was constructed from the 1.839kb SphI-XmnI and 1.946 XmnI-EcoRI fragments containing *EAF1* inserted between the SphI and EcoRI sites of YCplac33; pQZ3 contains the 1.77kb SphI-EcoRI fragment containing *RTT109* cloned between the corresponding sites of YCplac33; pQZ4 contains the 1.535 kb SphI-NruI and 1.799kb NruI-XmaI fragments containing WT *SAS3* inserted between the SphI and XmaI sites of YCplac33; and pQZ5 contains the 1.753 kb SphI–SacI fragment containing *YNG2* cloned between the corresponding sites in YCplac33. pHQ2142 (pFA6a-FRB-natMX4) was constructed by replacing the BglII-EcoRV *HIS3MX6* fragment of pFA6a-FRB-His3MX6 (from Euroscarf p30579) with the BglII-EcoRV *natMX4* fragment from pFA6-natMX4 (19).

Western blot analysis

Western analysis of yeast whole cell extracts prepared under denaturing conditions using trichloroacetic acid was conducted as described previously (20) using NuPAGE Bis–Tris gels and the following antibodies. Commercially available antibodies were employed to detect histone H3 (ab1791, Abcam), acetylated H3 (H3-ac) (06-599, Sigma), histone H4 (04-858, Sigma), and acetylated H4 (H4-ac) (06-866, Sigma). The H3-ac antibodies were raised against a human H3 peptide acetylated at the N-terminus. The immunogen for the H4-ac antibodies was an acetylated peptide corresponding to amino acids 2–19 of *Tetrahymena* H4 [AGGAcKGGAcKGMGAcKVGAAcKRHS-C], acetylated on lysines 5, 8, 12 and 16. Antibodies prepared in-house were used to detect Gcn4, Gcd6 or Hcr1.

ChIP-seq analysis

All ChIP-seq experiments conducted are summarized in Supplementary Table S1. WT and mutant strains were cultured in synthetic complete medium lacking isoleucine and valine (SC-Ilv) to A_{600} of 0.6–0.8 and sulfometuron methyl (SM) was added at 1 μg/ml for 25 min to induce Gcn4 synthesis prior to treating cells with formaldehyde, as previously described (3). For anchor-away strains, yeast cells were cultured in SC-Ilv to A_{600} of 0.3–0.4, rapamycin was added to 1 μg/ml and incubation continued for 1.5 h, after which SM was added as above before formaldehyde treatment. ChIP-seq using sonication for chromatin fragmentation was conducted (21) with modifications described in (3) using polyclonal antibodies against H3, H3-ac, and H4-ac (described above), TBP (a generous gift from Joseph Reese) or Gcn4 (22), and monoclonal antibodies against Rpb3 (NeoClone, W0012), Rpb1 (8WG16 from Biolegend, 664906) or the myc epitope (Mouse Monoclonal Antibody 9E10 from Roche 11667203001). H3 ChIP-seq using micrococcal nuclease to fragment chromatin was conducted as in (6). Supplementary Figure S1A indicates that the fragment length distributions of sonicated chromatin samples were similar among replicates for representative chromatin samples. DNA libraries for Illumina paired-end sequencing were prepared using the DNA Library Prep Kit for Illumina from New England Biolabs (E7370L).

Paired-end sequencing (50 nt from each end) was conducted by the DNA Sequencing and Genomics core facility of the NHLBI, NIH. Sequence data were aligned to the SacCer3 version of the genome sequence using Bowtie2 (23) with parameters *-X 1000 –very-sensitive*, to map sequences up to 1 kb with maximum accuracy. PCR duplicates from ChIP-seq data were removed using *samtools rmdup*. Numbers of aligned paired reads from each ChIP-seq experiment and correlation coefficients for genome-wide occupancy profiles of the different replicates are summarized in Supplementary Table S1. Raw genome-wide occupancy profiles for H3, Rpb3, Gcn4, TBP, and myc-tagged proteins were computed using the coverage function in R. To allow the comparison between different samples, each profile was normalized to an average of 1 for each chromosome. Heat maps showing alignments of multiple loci were generated in R using custom scripts (https://github.com/rchereji/bamR). To visualize specific loci, *BigWig* files of samples were loaded in the Integrative Genomics Viewer (IGV) (24). Transcript end coordinates (TSS and TTS) were obtained from (Pelechano *et al.*, 2013).

For spike-in normalization of Rpb1 ChIP-seq data, *S. pombe* chromatin was prepared from strain ED668 (Bioneer) using the same procedure employed for *S. cerevisiae*, aliquoted, and stored at –80°C. Prior to immunoprecipitating Rpb1, aliquots of *S. pombe* chromatin were added to each *S. cerevisiae* chromatin sample being analyzed in parallel, corresponding to 10% of the *S. cerevisiae* chromatin in the samples based on the DNA concentrations of the chromatin preparations. As described fully in File S3, the average number of total Rpb1-immunoprecipitated reads mapping to the *S. pombe* genome across the samples was determined and used to calculate the normalization factor for each sample as the average number of total *S. pombe* reads divided by the number of Rpb1-immunoprecipitated reads mapping to the *S. pombe* genome for that sample. The observed reads mapping to the *S. cerevisiae* genome for each sample were multiplied by the normalization factor to yield the spike-in normalized reads for each *S. cerevisiae* gene. Raw genome-wide occupancy profiles for Rpb1 were computed using the coverage function in R, wherein each profile was set with the same total OCC to allow the comparison between different samples (control and treatments), using the custom R script (https://github.com/hzhanghenry/OccProR). Spike-in normalization of H3-ac and H4-ac was conducted similarly using *S. pombe* chromatin, calculating normalization factors from the total number of reads mapped to the *S. pombe* genome that were used to normalize the numbers of reads mapped to each nucleotide in the *S. cerevisiae* genome, as described in Files S11. H3-ac/H3 and H4-ac/H3 ratios were calculated by dividing the spike-in normalized H3-ac or H4-ac occupancies averaged over the [–1,NDR,+1] intervals by the averaged relative H3 occupancies for the same intervals calculated from H3 ChIP-seq experiments conducted in parallel with those examining acetylated histone occupancies described in File S11.

TBP occupancies at the TBP peaks of SM-induced genes were calculated as previously described (12) using the peak coordinates of the 116 TBP peaks listed in Supplementary Table S5, except that a window of 100 bp surrounding the summit of each peak was evaluated. TBP occupancies at

the different groups of constitutive or RP genes were calculated by averaging the occupancies over the intervals –150 bp to +100 bp surrounding the TSSs. Gcn4 occupancies were quantified for 117 Gcn4 peaks located 5' of Gcn4 target genes (25), averaging the occupancies over the –100 bp to 100 bp intervals surrounding the Gcn4 motifs, listed in Supplementary Table S6. Occupancies of Spt7-myc, Eaf1-myc, and Srb6-myc were corrected using the data obtained by parallel ChIP-seq analyses of the untagged isogenic WT or mutant strains, as described previously (12).

RESULTS

Disruption of NuA4 and deletion of *GCN5* confer comparable defects in promoter nucleosome eviction at SM-induced genes

Previously, we reported that the HAT Gcn5 promotes both eviction of promoter nucleosomes and transcriptional activation at a large cohort of genes induced by starvation for the amino acids isoleucine and valine achieved using SM, which is mediated primarily by Gcn4 (3). We began here by confirming the role of Gcn5 in nucleosome eviction at SM-induced genes by ChIP-seq analysis of histone H3 in cells deleted of *GCN5*. As expected, the *gcn5Δ* strain exhibits a modest slow-growth (Slg$^-$) phenotype on synthetic complete (SC) medium lacking SM (Supplementary Figure S2A); and shows reduced levels of bulk H3 acetylated at its N-terminus (H3-ac), in both the presence and absence of SM, compared to the WT strain (Supplementary Figure S2E, H3-ac versus H3). The reduction in H3-ac by *gcn5Δ* is exacerbated by SM treatment (Supplementary Figure S2E, +SM vs -SM) but the underlying mechanism for this last finding remains to be explored. Both the Slg$^-$ phenotype and reduction in H3-ac conferred by *gcn5Δ* were complemented by plasmid-borne WT *GCN5* (Supplementary Figure S2A and E). Importantly, deletion of *GCN5* did not noticeably alter the induction of Gcn4 protein by SM treatment (Supplementary Figure S2E, Gcn4).

Our previous ChIP-seq analysis of Pol II subunit Rpb3 identified 204 genes showing ≥2-fold induction of Rpb3 occupancies on SM treatment; and ChIP-seq of histone H3 revealed that 70 of these SM-induced genes display a marked reduction in nucleosome occupancies in their promoter regions. As expected, our current H3 ChIP-seq data revealed reduced H3 occupancies in the promoter regions of four well-studied Gcn4 target genes belonging to the group of 70 SM-induced genes, *HIS4, CPA2, ARG4* and *ARG7,* on SM-induction of WT cells (Supplementary Figure S3A(i)–(iv), row 1, light versus dark colors, data within dashed lines). As the results of H3 ChIP-seq analysis were highly reproducible among three biological replicates of the *gcn5Δ* mutant and isogenic WT strains (Supplementary Figures S1B and S3B; Supplementary Table S1), we combined the replicate datasets for each condition in performing downstream analyses. Averaging results for all 70 SM-induced genes revealed reductions in the mean H3 occupancies in response to SM treatment (WT_I versus WT_U) in the DNA regions spanning the average consensus positions of the –1_Nuc, NDR and +1_Nuc (Supplementary Figure S4A), using the sequence coordinates for these regions we had defined previously by sequencing nucleosomes released from chromatin by micrococcal nuclease digestion (MNase-Seq) (3). Using these same coordinates to calculate the average H3 occupancy per nucleotide across the intervals spanning the –1_Nuc, NDR, and +1_Nuc regions (dubbed [-1,NDR,+1]), we observed marked reductions in median occupancies of H3 in the promoters of the group of 70 genes on SM-treatment of WT cells (Supplementary Figure S4B). (In these and other notched box plots, non-overlapping notches in adjacent plots indicate that the two medians differ significantly with ≥95% confidence. *P*-values from Mann–Whitney *U* tests of the statistical significance of the difference between groups is also frequently indicated with asterisks.) As expected from our previous findings (3,6), the remaining 134 among all 204 SM-induced genes exhibit smaller, but still highly significant, reductions in median H3 occupancies on SM treatment of WT (Supplementary Figure S4B).

As expected, deleting *GCN5* significantly diminished the reduction in the averaged H3 occupancies across the promoter regions of both groups of 70 and 134 induced genes evoked by SM treatment (Supplementary Figure S4A and B, $gcn5\Delta_I$ versus WT_I). These changes in median H3 occupancies were observed reproducibly for all SM-induced genes in the biological replicates of the WT_I, WT_U and $gcn5\Delta_I$ strains (Supplementary Figure S1B). In contrast, *gcn5Δ* had little effect on promoter H3 occupancies in cells untreated with SM (Supplementary Figure S4A, $gcn5\Delta_U$ versus WT_U), indicating that Gcn5 makes little contribution to basal nucleosome occupancies at SM-induced genes.

The effects of *gcn5Δ* on H3 eviction at individual members of the groups of 70 and 134 genes were visualized by constructing heat maps of H3 occupancies in the regions surrounding the +1_Nucs, with the genes sorted according to the previously determined Pol II occupancies averaged across the CDSs in SM-treated WT cells, as measured by ChIP-seq analysis of Rpb3 (3) (Supplementary Figure S4C(i)). The difference map in Supplementary Figure S4C(ii) shows the magnitude of H3 eviction in SM-treated versus untreated WT cells as different shades of blue for each gene. As expected, the amount of H3 eviction in WT is considerably smaller for the 134 genes (*lower* sector) versus the 70 induced genes (*upper* sector) (Supplementary Figure S4C(ii)). The difference map in Supplementary Figure S4C(iii) depicts the increases in H3 occupancy (as yellow, orange, or red hues) in *gcn5Δ* versus WT cells under inducing conditions for the same ranking of genes. Note that *gcn5Δ* confers increased occupancies in the vicinity of both the –1_Nucs and +1_Nucs for most of the group of 70 induced genes (Supplementary Figure S4C(iii)), but it generally confers smaller effects on H3 eviction at the 134 induced genes (Supplementary Figure S4C(iii), *lower*).

We noticed that H3 occupancies were lower in induced *gcn5Δ* cells compared to uninduced WT cells for the group of 70 genes (Supplementary Figure S4A, B), suggesting that appreciable H3 eviction still occurs in the absence of Gcn5. Our previous finding that Gcn4 recruits the HAT complex NuA4 to *ARG1* during SM-induction (14), led us to inquire whether the HAT activity of NuA4 also participates in H3 eviction, and mediates the nucleosome eviction on SM-induction evident in *gcn5Δ* cells (Supplementary Figure S4A, B). Because the catalytic subunit of NuA4 (Esa1) is essential, we examined the effects of deleting non-essential

NuA4 subunits Eaf1 or Yng2. Eaf1 is important for the integrity of NuA4 (14,26,27) and is required for recruitment of other NuA4 subunits to the *ARG1* UAS region by Gcn4, possibly by tethering the Tra1 subunit to the rest of NuA4 (14), as Tra1 is a known target of the Gcn4 activation domain (15). Yng2 resides with Esa1 and Epl1 in both NuA4 and the NuA4 subcomplex picNuA4, and enhances Esa1 HAT activity (28). We verified that deletions of *EAF1* and *YNG2* confer reductions in acetylated H4, which were complemented by the corresponding WT alleles; and we established that *eaf1Δ* and *yng2Δ* did not impair induction of Gcn4 protein on SM-treatment (Supplementary Figure S2F, G). Similar to our findings on *gcn5Δ* in reducing H3Ac levels, the effects of *eaf1Δ* and *yng2Δ* on bulk H4Ac levels are exacerbated by SM treatment (Supplementary Figure S2F, G); but the underlying mechanism is unknown. The *eaf1Δ* and *yng2Δ* mutations conferred Slg$^-$ phenotypes, greater than those given by *gcn5Δ,* which were fully complemented by the WT alleles (Supplementary Figure S2A–C).

Importantly, deletion of *EAF1* confers increased H3 promoter occupancies on SM-induction *on par* with the effect of *gcn5Δ* for the SM-induced genes. First, H3 occupancy difference heat maps reveal that *eaf1Δ* confers increased H3 occupancies similar in degree for the group of 70 SM-induced genes, while affecting an even greater proportion of the group of 134 genes, compared to those described above for *gcn5Δ* and shown again for comparison in Figure 1A (panels (ii) versus (i)). Second, *eaf1Δ* confers increases in median H3 occupancies similar to those given by *gcn5Δ* for the group of 70 genes, and exceeding the effect of *gcn5Δ* for the 134 genes (Figure 1B(i)–(ii)). In fact, the median H3 occupancies in induced *eaf1Δ* cells is indistinguishable from those seen in uninduced WT cells for the group of 134 genes (Figure 1B(ii)). This last finding led us to consider whether NuA4 also contributes to basal promoter nucleosome occupancies at the SM-inducible genes. Indeed, H3 ChIP-seq analysis of uninduced cells revealed that, unlike *gcn5Δ, eaf1Δ* confers significantly higher basal median H3 occupancies for the group of 134 genes (Figure 1C(ii)). Together, these findings suggest that NuA4 and Gcn5 are required almost equally for efficient eviction of promoter nucleosomes at the SM-induced genes when Gcn4 is induced, and that NuA4 also functions in this process under basal conditions.

Elimination of NuA4 subunit Yng2 also impaired promoter nucleosome eviction at the SM-induced genes, but generally had a smaller effect compared to *eaf1Δ.* The *yng2Δ* mutation was examined in a strain background (BY4742) regarded as largely isogenic to the WT strain analyzed above (BY4741) except for the allelic differences of *MATα* versus *MATa*, *lys2Δ-0* versus *LYS2*, and *MET15* versus *met15Δ-0* (29). SM-treatment of WT strain BY4742 evoked extensive H3 eviction in the promoters of the groups of 70 and 134 genes (Figure 1A(iii)) comparable to that shown above for WT strain BY4741 (Supplementary Figure S4C(ii)). Deletion of *YNG2* conferred a moderate increase in H3 occupancies (yellow-orange hues) that was relatively greater for the group of 70 genes versus 134 SM-induced genes (Figure 1A(iv)); and was substantially smaller overall than that given by *eaf1Δ* (Figure 1A(ii)) for both groups of genes. Furthermore, while *yng2Δ* produced significant increases in median H3 occupancies for the SM-induced genes, the fold-increases compared to the isogenic WT strain, of 1.1- to 1.25-fold, were smaller than those given by *eaf1Δ* of 1.2- to 1.6-fold, for the two groups of genes (Figure 1B(i)–(ii)). Unlike the findings above for *eaf1Δ,* H3 occupancies in the *yng2Δ* strain under inducing conditions remained well below those in uninduced WT cells (Figure 1B(i)–(ii)). Moreover, *yng2Δ* did not increase the median H3 occupancies in uninduced cells (Figure 1C(i)–(ii)). Thus, it appears that eliminating Yng2 confers a smaller defect in promoter nucleosome eviction at the SM-induced genes, in induced and uninduced cells, compared to disrupting NuA4 by eliminating Eaf1.

Considering that many SM-induced genes are direct targets of Gcn4, exhibiting increased Gcn4 occupancies in the NDRs on SM-induction of WT cells (25), we examined whether reductions in promoter nucleosome eviction conferred by *gcn5Δ, eaf1Δ* or *yng2Δ* might be secondary effects of reduced Gcn4 occupancies at its target genes. ChIP-Seq analysis of Gcn4 revealed the expected induction of occupancies averaged over all 117 Gcn4 binding peaks located within NDRs on SM treatment of WT (Supplementary Figure S5A). The *gcn5Δ* mutation conferred an increase, rather than decrease, in both averaged and median Gcn4 occupancies under inducing conditions; whereas *eaf1Δ* conferred a modest but significant reduction in Gcn4 occupancies (Supplementary Figure S5A, B). Thus, the defects in promoter nucleosome eviction conferred by *gcn5Δ* are clearly not associated with diminished Gcn4 binding; whereas reduced Gcn4 occupancies might contribute somewhat to the diminished nucleosome eviction observed in *eaf1Δ* cells at SM-induced genes.

Eliminating Rtt109 or Sas3 has little effect on promoter nucleosome eviction at SM-induced genes

We examined next the effect of eliminating Rtt109, which acetylates K56 in the globular domain of histone H3 (30); or Sas3, which acetylates H3 as a subunit of the NuA3 HAT complex (31). The *rtt109Δ* strain exhibits a Slg$^-$ phenotype and somewhat diminished levels of bulk acetylated H3, both of which were complemented by plasmid-borne *RTT109* (Supplementary Figure S2D, H); however, we observed no effects of *sas3Δ* on either cell growth or histone acetylation.

In comparison to *eaf1Δ*, the *rtt109Δ* and *sas3Δ* mutations had smaller effects on promoter H3 occupancies for the SM-induced genes under inducing conditions (Supplementary Figure S6A(i)–(iii)), producing a significant increase in median H3 occupancies only in the case of *rtt109Δ* and limited to the 70 induced genes (Supplementary Figure S6B(i)–(ii)). Examining the H3 difference map for *rtt109Δ,* reveals that the increased H3 occupancies for these genes are concentrated in the -1_Nuc regions (Supplementary Figure S6A (ii), *upper*). In contrast to *eaf1Δ, rtt109Δ* and *sas3Δ* had no significant effects on median promoter H3 occupancies for the SM-induced genes under basal conditions (Supplementary Figure S6C(i)–(ii)). Thus, among the four HATs we examined, only Gcn5 and NuA4 make strong

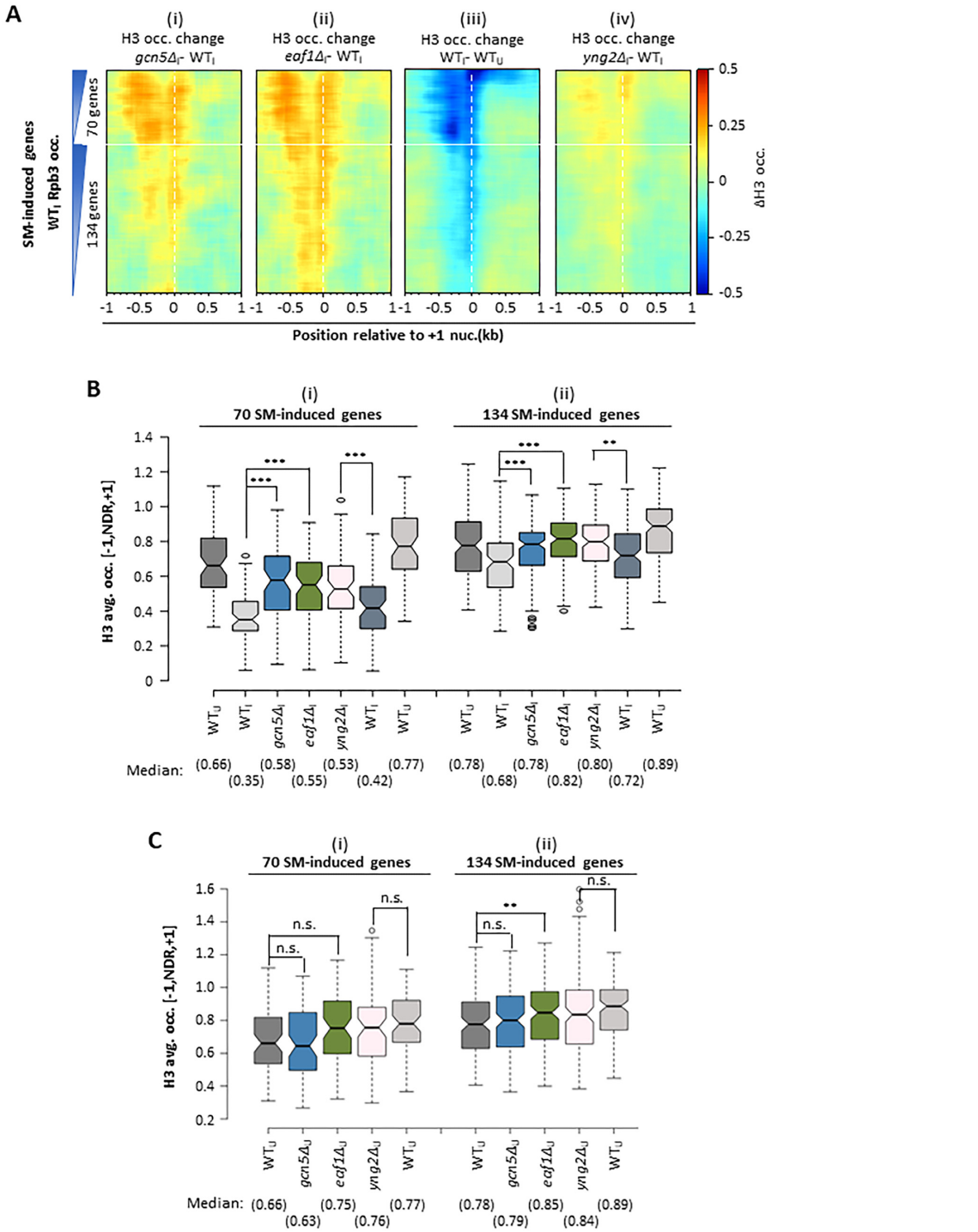

Figure 1. Disruption of NuA4 by deletion of *EAF1* is *on par* with deletion of *GCN5* in reducing promoter nucleosome eviction at SM-induced genes. (**A**) Heat map depictions of differences in H3 occupancies in WT cells induced by SM treatment (WT_I) versus untreated (uninduced) WT cells (WT_U) (iii), or between the indicated mutant and WT strains (described in Supplementary Figure S1A-C) grown under inducing conditions (i), (ii), (iv), calculated from the combined H3 ChIP-seq data for the 204 SM-induced genes, divided between 70 (upper) and 134 (lower) SM-induced genes, plotted relative to the +1_Nuc dyad and color-coded as shown in the scale to the right of panel (iv). Genes in each group were sorted by their average Rpb3 occupancies over the CDS in WT_I cells (3) as summarized schematically on the far left. (**B**) Notched box plots of H3 occupancies per nucleotide in the [−1,NDR,+1] regions calculated from combined ChIP-seq data for each strain in (A) for the 70 and 134 SM-induced genes. Note that the *yng2Δ* mutant was compared to its isogenic WT strain (in cols. 6–7), which differs from the WT strain isogenic to the *gcn5Δ* and *eaf1Δ* strains examined in parallel with the latter two mutants (cols. 1–2). Each box depicts the interquartile range containing 50% of the data, intersected by the median; the notch indicates a 95% confidence interval (CI) around the median. If the notches of two plots do not overlap, there is 95% confidence that the true medians of the two distributions differ. Asterisks signify significant differences between the two groups connected by brackets according to the Mann–Whitney *U* test: ***$P < 0.001$; **$P < 0.01$, *$P < 0.05$. Median values are given in parenthesis below the column labels. (**C**) Notched box plots of H3 occupancies per nucleotide in the [−1,NDR,+1] region as in (B) except for cells grown in uninducing conditions.

contributions to promoter nucleosome eviction at the SM-induced genes.

NuA4 acts more broadly than Gcn5 in evicting promoter nucleosomes genome-wide

Having found that deleting *EAF1* increased basal promoter nucleosome occupancies in uninduced cells at many SM-induced genes (Figure 1C), we asked whether this defect could be observed more broadly at genes that are not induced by SM. To this end, we interrogated the H3 occupancies for a group of 3619 genes that showed <1.2-fold increases in Rpb3 occupancies on SM induction (3) and, hence, are expressed more constitutively than the 204 SM-induced genes analyzed above. Examining H3 difference heat-maps (sorted as above according to Rpb3 occupancies in WT_I cells) revealed that these genes exhibit only small reductions in promoter H3 occupancies on SM-treatment of WT cells (Figure 2A(i)), as expected from their constitutive expression. The *gcn5Δ* mutation confers marked increases in promoter H3 occupancies only at the most highly expressed subset of genes located at the top of the heat-map (Figure 2A(ii)). Importantly, *eaf1Δ* confers relatively larger increases in promoter H3 occupancies compared to *gcn5Δ* for nearly all constitutively expressed genes, including those at the top of the map most affected by *gcn5Δ* (Figure 2A(iii)). As observed for the SM-induced genes, *yng2Δ* confers a considerably smaller defect in H3 eviction for the constitutive genes than observed for *eaf1Δ* (Figure 2A(v) versus (iii)), or even for *gcn5Δ* (panel v versus ii). These trends are borne out by comparing the median promoter H3 occupancies in the three mutant strains, with *eaf1Δ* conferring a significantly larger increase versus WT_I cells (1.17-fold) compared to *gcn5Δ* (1.08-fold); and with *yng2Δ* producing the smallest increase among the three mutations (1.05-fold compared to its isogenic WT strain) under inducing conditions (Figure 2B). Under non-inducing conditions, *eaf1Δ* again produced a greater increase in promoter H3 occupancies compared to *gcn5Δ* (1.08-fold versus 1.03-fold) (Figure 2C), indicating a greater role for NuA4 than Gcn5 in evicting promoter nucleosomes from the constitutively expressed genes. Surprisingly, *yng2Δ* confers lower rather than higher H3 occupancies in nonstarved cells (Figure 2C). The opposite effects of *yng2Δ* on H3 occupancies between starved and nonstarved cells, coupled with the similar effects of *eaf1Δ* between the two conditions, might indicate that picNuA4 (containing Yng2 but not Eaf1) functions more prominently in replacement rather than eviction of nucleosomes at constitutively expressed genes in non-starved cells; however, we are unaware of any previous observations that would support this speculation.

Finally, the *rtt109Δ* and *sas3Δ* mutations confer small, but significant increases in median promoter H3 occupancies for the 3619 constitutive genes, comparable to those conferred by *gcn5Δ* but decidedly smaller than those given by *eaf1Δ,* under both starvation and nonstarvation conditions (Supplementary Figure S7A–C). Thus, it appears that NuA4 plays the greatest role among the four HATs we examined in evicting promoter nucleosomes from the thousands of constitutively expressed genes.

NuA4 and Gcn5 make additive contributions to eviction and repositioning of promoter nucleosomes at both SM-induced and constitutively expressed genes

To determine whether NuA4 and Gcn5 function independently in promoter nucleosome eviction, we sought to determine whether eliminating one would confer increased promoter occupancies in mutant cells lacking the other HAT. As we could not construct a strain lacking both *GCN5* and *EAF1* owing to lethality of the double deletion (32), we resorted to examining the effects of conditionally depleting Eaf1 from the nucleus by 'anchor-away' (abbreviated below as AA) (33) from a strain lacking *GCN5.* To this end, WT and *gcn5Δ* strains were generated harboring an *FRB*-tagged allele of *EAF1* (dubbed *eaf1-AA*), an *FKBP12*-tagged allele of *RPL13A* encoding the cytoplasmic 'anchor' protein, and the *fpr1Δ* and *tor1-1* alleles that confer rapamycin (Rap) insensitivity of the TORC1 kinase complex (33). We similarly constructed WT and *eaf1Δ* strains containing the *FRB*-tagged *gcn5-AA* allele for nuclear depletion of Gcn5 in the presence and absence of *EAF1.* In addition, *gcn5Δ* and *eaf1Δ* strains containing *RPL13A-FKBP12, fpr1Δ* and *tor1-1,* but lacking an *FRB*-tagged allele were produced as controls to determine the effects of completely eliminating Gcn5 or Eaf1 in strains engineered for AA experiments (dubbed the AA background). Anchor-away of Eaf1 in the presence of Rap conferred a modest Slg^- phenotype in otherwise WT cells, but a more pronounced growth defect in the *gcn5Δ* strain (Supplementary Figure S8A(ii)). The Slg^- phenotype given by *eaf1-AA* on Rap treatment is weaker than that of *eaf1Δ* (Supplementary Figure S8A(ii)), suggesting incomplete nuclear depletion of Eaf1 by AA; which is not unusual with the AA approach (12,34). In contrast, the *gcn5-AA* allele conferred no discernible growth defects in both *EAF1* and *eaf1Δ* cells (Supplementary Figure S8A(ii)), suggesting that Gcn5 AA was largely ineffective. These interpretations were supported by Western analyses revealing an obvious reduction in H4-ac in Rap-treated *eaf1-AA*_I vs. WT_I cells (Supplementary Figure S8B), but little or no reduction in H3-ac in *gcn5-AA*_I cells (Supplementary Figure S8C). Accordingly, we focused on the *eaf1-AA* mutants that contain or lack *GCN5*.

ChIP-seq analysis of H3 was carried out as above except that all strains were cultured for 1.5h in the presence of Rap for AA before the addition of SM to induce Gcn4. Heat map analysis of the H3 occupancy changes in the WT, *gcn5Δ,* and *eaf1Δ* strains in the AA background produced results very similar to those described above in Figures 1 and 2 for the corresponding WT, *gcn5Δ,* and *eaf1Δ* strains, for both SM-induced and constitutive genes (Figure 3A(i), (ii), (iv)). Thus, *gcn5Δ* conferred a marked defect in H3 eviction for the 70 SM-induced genes, a smaller defect for the 134 induced genes, and a substantial defect only for the small subset of most highly expressed constitutive genes (Figure 3A(iv) *top, middle* and *bottom*). As observed above, the *eaf1Δ* mutation conferred H3 occupancy increases *on par* with the effects of *gcn5Δ* for the SM-induced genes, but relatively greater increases for the 3619 constitutive genes (Figure 3A(ii), *top, middle* and *bottom*). Thus, the differential effects of *gcn5Δ* and *eaf1Δ* on H3 occupancies were fully reproduced in the strains engineered for AA.

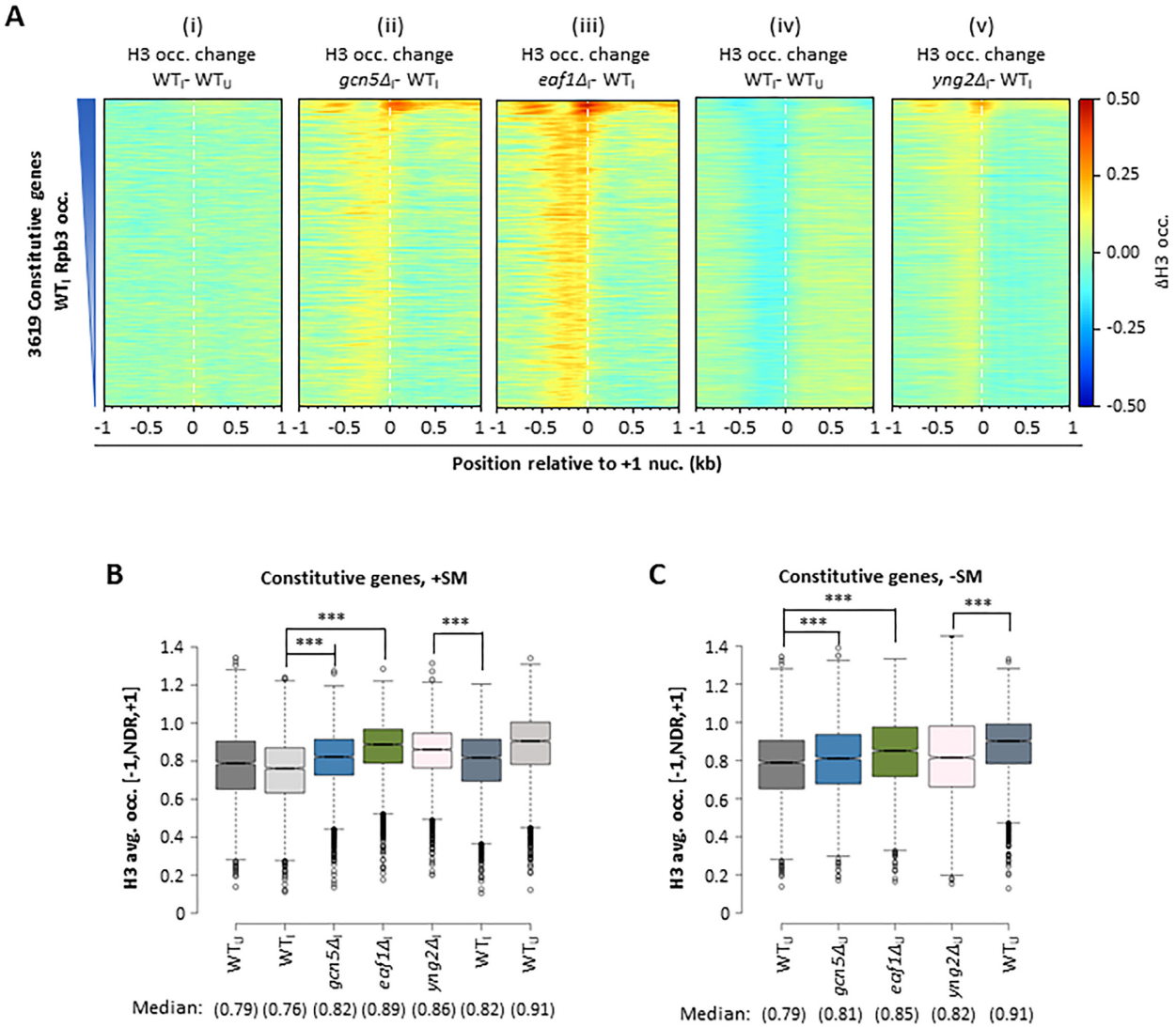

Figure 2. Disruption of NuA4 by deletion of *EAF1* generally confers greater increases in promoter nucleosome occupancies at constitutively expressed genes compared to *gcn5*Δ. (**A**) Heat map depictions of differences in H3 occupancies on SM induction of WT cells (i) or (iv), or between mutant and WT cells (described in Supplementary Figure S1A–C) under inducing conditions (ii), (iii) or (iv), calculated from the combined H3 ChIP-seq data for the 3619 constitutive genes, plotted relative to the +1_Nuc dyad and color-coded as shown in the scale to the right of panel (v). Genes were sorted by their average Rpb3 occupancies over the CDS in WT$_I$ cells (3) as summarized schematically on the far left. (**B**, **C**) Notched box plots of H3 occupancies per nucleotide in the [−1,NDR,+1] regions calculated from combined ChIP-seq data for each strain in (A) for the constitutive genes under inducing conditions (except for WT shown also for uninducing conditions (B), or under non-inducing conditions (C). Asterisks signify significant differences between the two groups connected by brackets according to the Mann–Whitney *U* test: ***$P < 0.001$; **$P < 0.01$, *$P < 0.05$. Median values are given in parenthesis below the column labels.

For the majority of genes in all three groups, AA of Eaf1 conferred relatively small increases in H3 occupancy, considerably less than conferred by *eaf1Δ* (Figure 3A(ii)-(iii). However, *eaf1-AA* clearly exacerbated the eviction defects in *gcn5Δ* cells for all three sets of genes (Figure 3A(iv)–(v)). The additive effects of the *eaf1-AA* and *gcn5Δ* mutations is also evident in the significantly larger median H3 occupancies in the [–1,NDR,+1] intervals in the *eaf1-AA gcn5Δ* double mutant compared to the *gcn5Δ* single mutant for both the SM-induced and constitutively expressed genes (Figure 3B, C). Thus, although apparently incomplete, nuclear depletion of Eaf1 by AA was effective enough to reveal that NuA4 functions in H3 eviction even in cells lacking Gcn5 and, hence, can contribute to promoter nucleosome eviction independently of Gcn5.

Because the TSS generally resides within the +1_Nuc (35), the latter may impose a barrier to PIC assembly that can be overcome by its repositioning (4,5,36) in addition to its eviction from DNA. Indeed, we showed previously that the +1_Nuc is repositioned downstream at SM-induced genes in a manner involving both SWI/SNF and RSC (6). Hence, we asked next whether Gcn5 and NuA4 contribute to this aspect of promoter nucleosome remodeling. To examine changes in nucleosome locations, we conducted H3 ChIP-seq analysis of fragments generated from cross-linked chromatin by digestion with MNase (H3 MNase-ChIP-

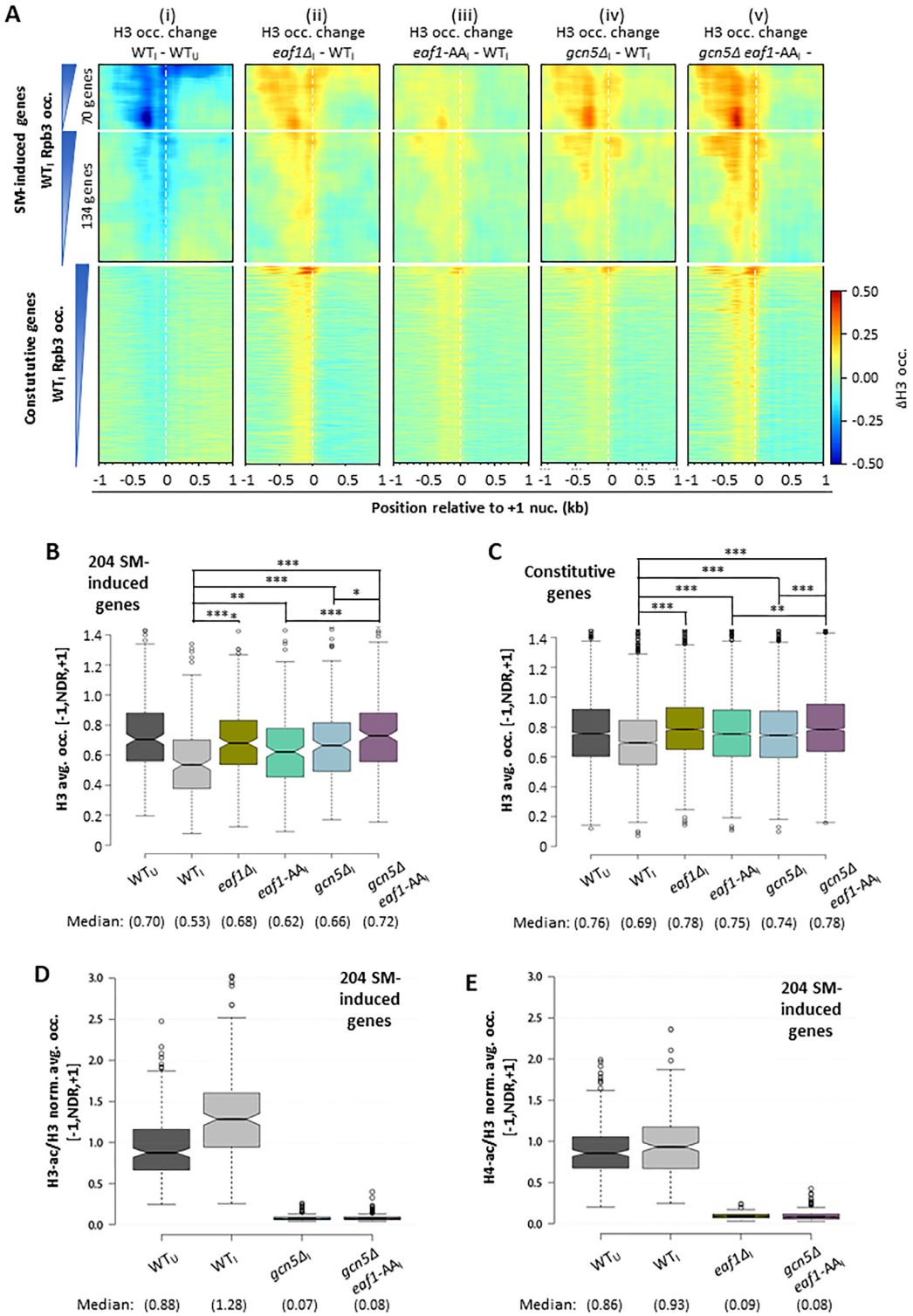

Figure 3. Additive effects of nuclear depletion of Eaf1 by anchor-away and deletion of *GCN5* in impairing eviction of promoter nucleosome occupancies at both SM-induced and constitutively expressed genes. (**A**) Heat maps of H3 occupancy differences on SM induction of WT cells (i), or between mutant and WT cells (for strains engineered for anchor-away described in Supplementary Figure S8A) under inducing conditions (ii)-(v), for the three gene sets indicated on the left, sorted by their WT $Rpb3_I$ occupancies and color-coded as in the scale to the right of panel (v). (**B**, **C**) Box plots of H3 occupancies in the [–1,NDR,+1] intervals for the indicated strains (in A) for the 204 SM-induced genes (B) or the 3619 constitutive genes (C), treated as in (A). All strains were treated with Rapamycin to induce nuclear depletion of Eaf1 (in the two *eaf1-AA* strains) and subsequently treated with SM for inducing conditions. (**D**) Elimination of Gcn5 or Eaf1 strongly decreases promoter nucleosomes acetylated on H3 or H4, respectively, at the 204 SM-induced genes. Box plots of spike-in normalized H3-ac occupancies normalized to total H3 occupancies, expressed relative to the average H3-ac/H3 ratio for all 5403 genes determined in the WT_U strain, averaged over the [–1,NDR,+1] intervals for the 204 SM-induced genes. (**E**) same as (D) except for spike-in normalized H4-ac occupancies normalized to total H3 occupancies, expressed relative to the average H4-ac/H3 ratio for all 5403 genes determined in the WT_U.

seq) rather than by sonication. To quantify nucleosome shifts, we plotted the mid-points of the immunoprecipitated nucleosome-size fragments, which approximate the positions of the nucleosome dyads. In agreement with our previous findings (6), averaging the dyad densities for all 204 SM-induced genes revealed a downstream shift in the +1_Nuc and an upstream shift of the –1_Nuc, thereby widening the NDR, on SM treatment of WT cells (Figure 4A(i)–(ii)). Examining the dyad positions at each gene individually revealed median shifts of +11 and –6 bp for the +1_Nuc and –1_Nuc, respectively, and a median increase in NDR width of 18 bp, on induction of these genes (Figure 4B(i), –1, +1), all in good agreement with our previous findings (6). Average plots showed that *gcn5Δ* and *eaf1Δ* partially reverse the shifts in position of both the +1_Nuc and –1_Nuc under inducing conditions (Figure 4A(i)–(ii)), narrowing the NDR from its length in WT_I cells by 3 or 4.5 bp, respectively (Figure 4B(ii)–(iii), width changes). While these shifts are modest, we observed a greater NDR narrowing of 8bp in the *gcn5Δ eaf1-AA* double mutant, which exceeded that given by either single mutation in the strains engineered for AA (Figure 4C(iv) versus (ii)–(iii), width changes). The effects of *gcn5Δ* and *gcn5Δeaf1-AA* in narrowing NDRs from those found in WT_I cells is illustrated for six SM-induced genes in Supplementary Figure S9. Interestingly, the *yng2Δ* mutation affecting NuA4 led to a greater NDR narrowing compared to *eaf1Δ* at the 70 induced genes, comparable in degree to that found previously for *snf2Δ* (6) (Supplementary Figure S10C).

In keeping with their lower Pol II induction ratios, the constitutive genes show a relatively smaller NDR widening on induction of WT cells of only 9bp (Supplementary Figure S10A(i)) versus 18 bp for the 204 induced genes (Figure 4B(i)). Importantly, *eaf1Δ* nearly reverses the NDR widening observed in WT cells (Supplementary Figure S10A (iii) versus (i)), and *gcn5Δ* and *eaf1-AA* conferred additive decreases in NDR width for the constitutive genes (Supplementary Figure S10B (iv) versus (ii)–(iii)). The *yng2Δ* mutation had a smaller, but still significant effect on NDR narrowing at the constitutive genes (Supplementary Figure S10D) compared to that noted for the 70 induced genes (Supplementary Figure S10C). Together, these results indicate that Gcn5 and NuA4 contribute to the repositioning of promoter nucleosomes that shifts the +1_Nuc downstream and widens the NDRs of both SM-induced and constitutively expressed genes, with NuA4 playing a greater role than Gcn5 at the constitutive genes.

NuA4 and Gcn5 promote H3 and H4 acetylation at promoters throughout the genome

Although the *gcn5Δ* and *eaf1Δ* mutations decreased acetylation in bulk chromatin (Supplementary Figures S2 and S8), we sought to determine if reductions in promoter nucleosomes occurred similarly in different gene groups by ChIP-Seq analysis of acetylated H3 and H4 conducted in parallel with total H3 on the same chromatin samples. Owing to the broad reductions in acetylated histones in these mutants (Supplementary Figure S2E, F), it was necessary to 'spike-in' *S. pombe* chromatin prior to immunoprecipitation and normalize the *S. cerevisiae* reads to the total number of reads mapped to the *S. pombe* genome for each sample. Calculating the ratios of normalized H3-ac or H4-ac to total H3 occupancies (to control for changes in nucleosome levels), we observed increased H3-ac/H3 and H4-ac/H3 ratios in the [-1,NDR,+1] promoter intervals of the 204 induced genes on SM treatment of WT cells (Figure 3D, E). Both *gcn5Δ* and *gcn5Δ eaf1-AA* mutants showed dramatically reduced levels of H3-ac/H3 (Figure 3D), and the *eaf1Δ* and *gcn5Δ eaf1-AA* strains showed the same effects for H4-ac/H3 (Figure 3E), for this gene group. Similar results were obtained for the ribosomal protein genes, shown below to be dependent on both NuA4 and Gcn5 for transcription, except that they display comparatively higher levels of acetylated H3 and H4 in WT_U cells and diminished rather than increased acetylation on SM treatment in WT_I vs WT_U cells (Supplementary Figure S11A, B). The group of all 5403 expressed genes also show declines in H3/H3-and H4-ac/H3 on SM-treatment and strong reductions in H3ac/H3 or H4ac/H3 ratios in the *gcn5Δ* and *eaf1Δ* mutants, respectively (Supplementary Figure S11C, D). Thus, Gcn5 and NuA4 are crucial for H3 and H4 acetylation in promoter nucleosomes, respectively, throughout the genome, in agreement with previous findings (16).

The simplest explanation for the effects of the *gcn5Δ* and *eaf1Δ* mutations in reducing nucleosome eviction is that it results from impaired nucleosome acetylation. If so, we might expect to find that the degree of the two defects are correlated. Supporting this possibility, the changes in H3ac/H3 ratios exhibit a significant moderate inverse correlation with the changes in total H3 occupancies in the two *gcn5Δ* mutants vs. WT for the 204 induced and RP genes (P values < 0.0003) (Supplementary Figure S11E and G, rows 1–2). The changes in H4ac/H3 ratios show a similar inverse correlation with changes in H3 occupancies in the *gcn5Δ eaf1-AA* double mutant vs. WT (Supplementary Figure S11F, G).

SAGA and NuA4 are recruited to most SM-induced genes

To provide evidence consistent with a direct role for Gcn5 and NuA4 in nucleosome acetylation and eviction at SM-induced genes, we conducted ChIP-seq analysis of myc-tagged versions of the Spt7 subunit of SAGA and Eaf1 of NuA4 in mutant and WT cells. Expression of the tagged proteins was not altered by the *gcn5Δ* or *eaf1Δ* mutations (Supplementary Figure S12A, B). Spt7-myc occupancies increased upstream of the TSS on SM treatment of WT cells at essentially all 70 induced genes and at many of the most highly expressed 134 induced genes (Supplementary Figure S12C(i), (ii)), whereas only low-level signals were observed in a parallel analysis of an isogenic untagged strain in the presence or absence of SM (Supplementary Figure S12D(i), (ii)). Correcting the *SPT7-myc* occupancies by those measured in the corresponding untagged strain revealed the recruitment of Spt7-myc in SM-induced cells at levels that generally scale with the induced Rpb3 occupancies at these gene sets (Figure 5A(i)–(ii)); and induction of Spt7-myc occupancies on SM induction was borne out by quantifying the occupancies in the NDRs (Figure 5B). Similar results were obtained for Eaf1-myc (Figure 5C(i), (ii); Figure 5D). Surprisingly, higher levels of Spt7-myc were

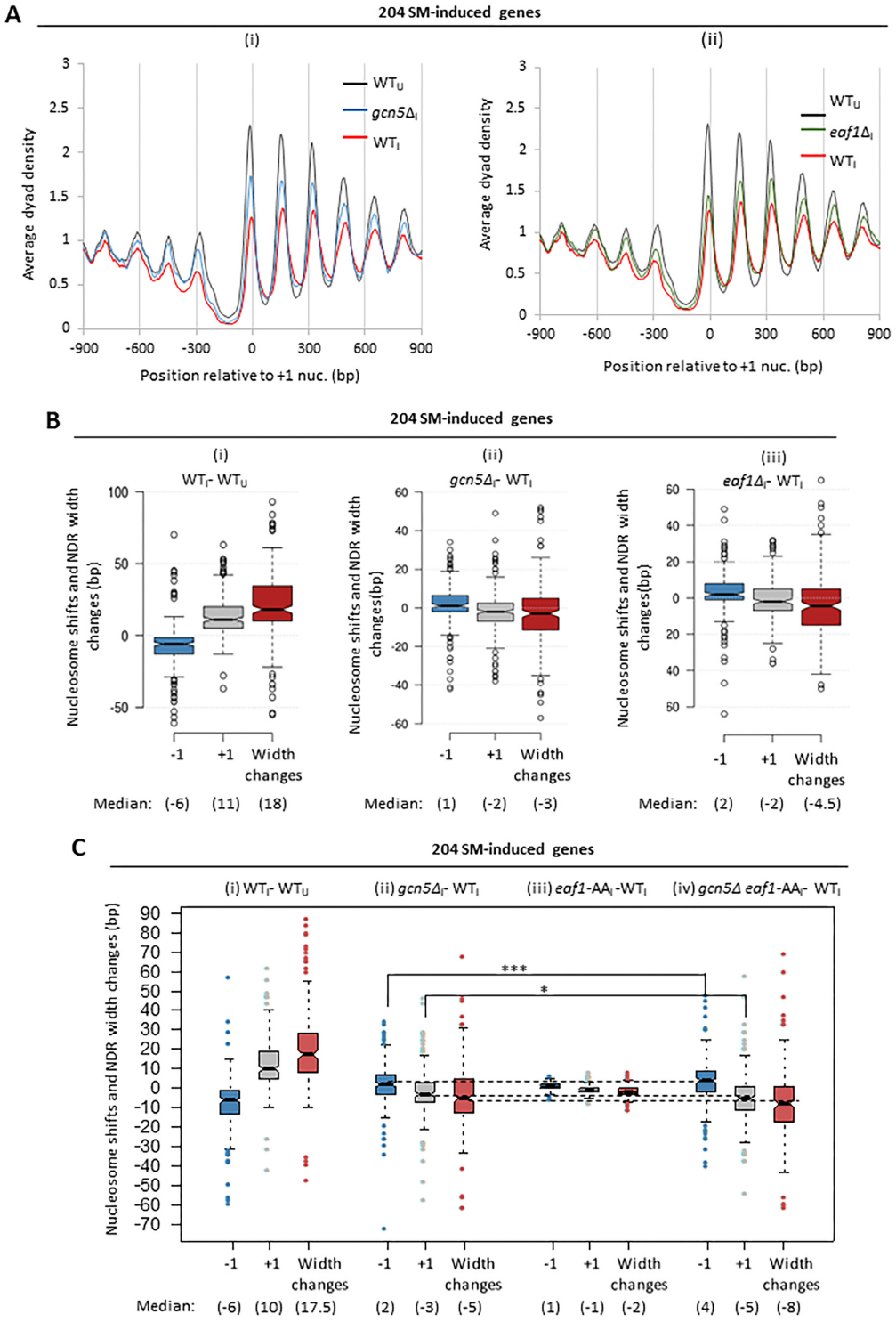

Figure 4. Additive effects of nuclear depletion of Eaf1 by anchor-away and deletion of *GCN5* in reversing the repositioning of promoter nucleosomes and NDR widening at SM-induced genes. (**A**) Average dyad densities of WT, *gcn5Δ* (i) or *eaf1Δ* (ii) mutant cells (using strains in Supplementary Figure S2A and B) for the 204 SM-induced genes calculated from MNase ChIP-seq data aligned to the +1_Nuc. Midpoints (dyads) of nucleosome-size sequences (between 120 and 160 bp) were determined with respect to the +1_Nuc and summed for the 204 genes. Average profiles were smoothed using a moving average filter with a span of 31 bp. The data were normalized internally to the average value for each data set. (**B**) Box plots depicting shifts in –1_Nuc or +1_Nuc positions or changes in NDR width for the 204 SM-induced genes, calculated from H3 MNase-ChIP-seq data by calculating changes in dyad peak positions, in WT_I versus WT_U cells (i), $gcn5\Delta_I$ versus WT_I cells (ii) or $eaf1\Delta_I$ versus WT_I cells. (**C**) Box plots depicting shifts in the –1_Nuc and +1_Nuc positions or changes in NDR widths for the 204 SM-induced genes, calculated as in (B) for strains engineered for AA (described in Supplementary Figure S8A) and treated with Rapamycin and SM as described in Figure 3: WT_I versus WT_U (i), $gcn5\Delta_I$ versus WT_I (ii), $eaf1\text{-}AA_I$ versus WT_I (iii), and $gcn5\Delta/eaf1\text{-}AA_I$ versus WT_I (iv). Asterisks signify significant differences between the two groups connected by brackets according to the Mann–Whitney *U* test: $^{***}P < 0.001$; $^{**}P < 0.01$, $^{*}P < 0.05$. Median values are given in parenthesis below the column labels.

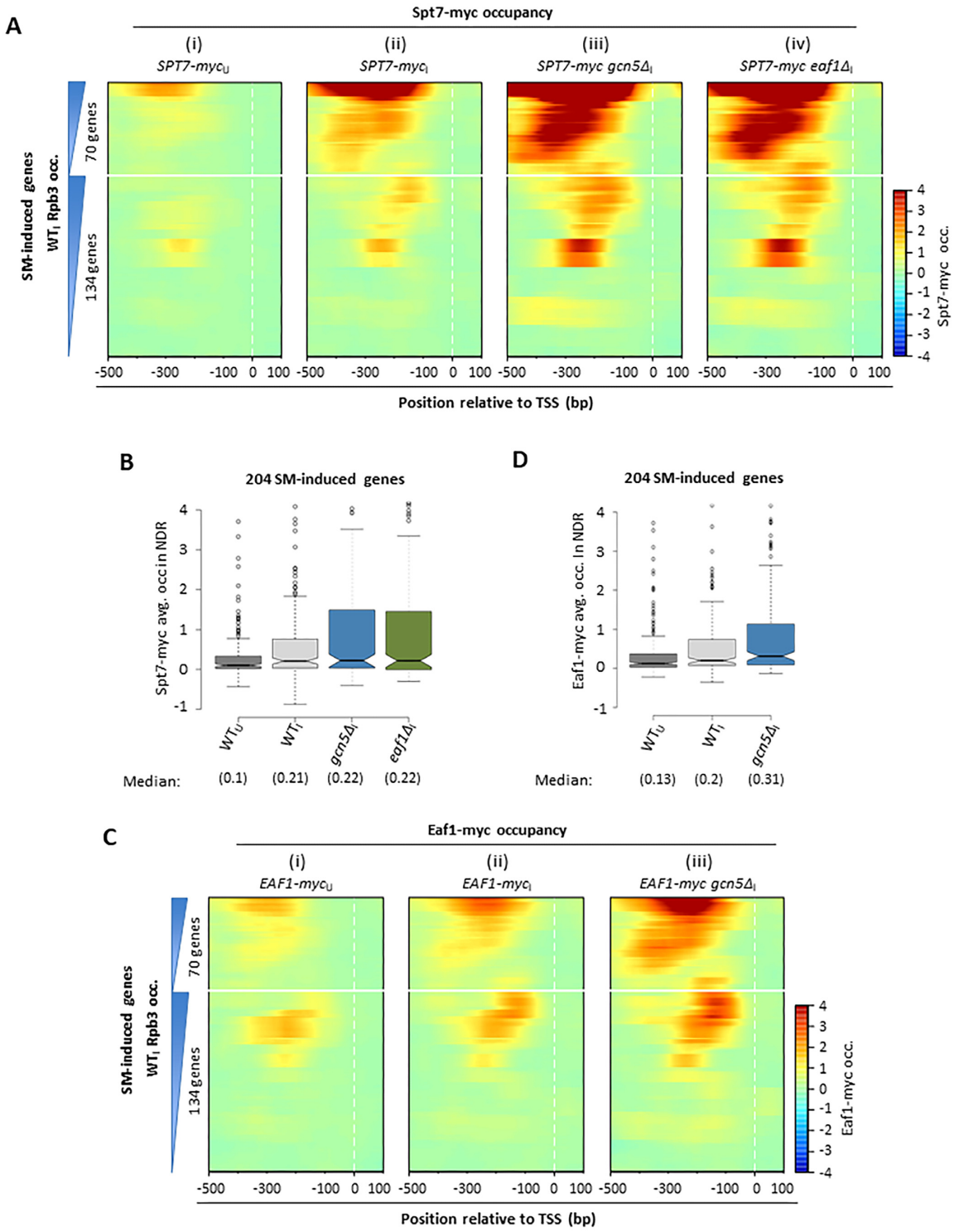

Figure 5. Evidence that SAGA (Spt7-myc) and NuA4 (Eaf1-myc) are recruited to the UASs at most of the 70 SM-induced genes during induction. (**A**, **B**) WT, *gcn5Δ* or *eaf1Δ* strains harboring *SPT7-myc* (H3587, H3591, and QZ25; described in Supplementary Figure S12B) and isogenic untagged strains (BY4741, F757 and H4311) were cultured as in Figure 1 and subjected to ChIP-seq using myc antibodies. Myc occupancies were corrected using the data from the isogenic untagged strains cultured identically. (A) Heat maps of corrected Spt7-myc occupancies for the indicated WT, *gcn5Δ,* or *eaf1Δ* cultures for the 204 SM-induced genes, divided between the 70 (upper) and 134 (lower) sets of SM-induced genes, plotted relative to the TSS and color-coded as shown in the scale to the right of panel (iv). Genes in each group were sorted by their average Rpb3 occupancies over the CDS in WT$_I$ cells (3) as summarized schematically on the left of (i). (**B**) Box plots of $\log_2$ corrected Spt7-myc occupancies averaged over the NDR for the SM-induced genes. Negative occupancies were obtained for a small number of genes owing to the correction for occupancies measured in the relevant untagged strain. (**C**, **D**) WT or *gcn5Δ* strains harboring *EAF1-myc* (H4268 and QZ21, described in Supplementary Figure S12A) and isogenic untagged strains (BY4741 and F757) were cultured and subjected to ChIP-seq using Myc antibodies as in (A, B). Myc occupancies were corrected using the data from the isogenic untagged strains cultured identically. Heat maps (C) and box plots (D) of $\log_2$ corrected Eaf1-myc occupancies are depicted as for Spt7-myc in (A, B).

observed at the same promoter locations for many of the induced genes in both *gcn5Δ*_I and *eaf1Δ*_I versus WT_I cells (Figure 5A (iii), (iv) versus (ii); Figure 5B). The *gcn5Δ* mutation also increased Eaf1-myc occupancies somewhat in SM-treated cells (Figure 5C(iii) versus (ii); Figure 5D). Together, these findings indicate that SAGA and NuA4 are both recruited to SM-induced genes in a manner increased on induction; and raise the possibility that negative feedback mechanisms limit recruitment of these HAT complexes, wherein reduced HAT function in the *gcn5Δ* and *eaf1Δ* mutants would lead to increased recruitment of the mutant HAT complexes.

At the 3619 constitutive genes, appreciable levels of Spt7-myc and Eaf1-myc were observed upstream of the TSS only for the most highly expressed subset of genes, and interestingly, were diminished rather than induced on SM-treatment of WT cells (Supplementary Figure S12E–F, panels (ii) versus (i)). This reduction, which is particularly pronounced for Eaf1-myc at the RP genes (Supplementary Figure S12G, col. 2 versus col. 1), might arise from increased competition with the highly expressed SM-induced genes for limiting SAGA and NuA4. The Spt7-myc occupancies appear to be slightly elevated in *gcn5Δ*_I versus WT_I cells (Supplementary Figure S12E, (iii) versus (ii)), as noted above for the SM-induced genes, suggesting that the putative feedback mechanism proposed above operates, at least for SAGA, at the most highly transcribed constitutively expressed genes.

Defects in promoter nucleosome eviction are associated with reduced Pol II occupancies in the HAT mutants

To evaluate the consequences of reduced promoter nucleosome eviction on transcription, we measured the occupancies of Pol II subunit Rpb1 across the CDS of all genes by ChIP-seq, employing a spike-in of *S. pombe* chromatin and an antibody (8WG16) that immunoprecipitates Rpb1 from both yeast species. Consistent with our previous results (3), the median Rpb1 occupancies increased markedly on SM treatment of WT cells for the set of 204 SM-induced genes (Figure 6A), reflecting their transcriptional induction. Importantly, both *gcn5Δ*$_I$ and *eaf1Δ*$_I$ cells display reduced median Rpb1 occupancies versus WT$_I$ cells (Figure 6A). While *eaf1-AA* had a smaller effect compared to *eaf1Δ,* it significantly exacerbated the reduction conferred by *gcn5Δ* in the double mutant (Figure 6A), consistent with additive effects of Gcn5 and NuA4 in promoting transcription of the SM-induced genes.

To compare the broader impacts of *gcn5Δ* and *eaf1Δ* on transcription, we examined their effects on transcription of the 3619 constitutive genes. As expected, these genes do not exhibit increased Rpb1 occupancies on SM treatment; rather, they display a reduced median Rpb1 occupancy (Figure 6B), which might result from increased competition for limiting factors imposed by the highly induced Gcn4 target genes, as suggested above for SAGA (Spt7-myc) and NuA4 (Eaf1-myc) occupancies. Interestingly, the *eaf1Δ* mutation conferred a larger reduction in the median Rpb1 occupancies at the constitutive genes than did *gcn5Δ* and combining *gcn5Δ* with *eaf1-AA* in the double mutant did not exacerbate the marked reduction given by *eaf1-AA* alone (Figure 6B)—both observations suggesting a minor role for Gcn5 in transcription of the constitutive genes.

To explore whether Gcn5 might have a greater impact on the more highly transcribed subset of constitutively expressed genes, we divided the 3619 constitutive genes into ten equal deciles according to their relative Rpb3 occupancies in WT$_I$ cells (3), from highest (decile D1) to lowest (D10) values. Examining promoter nucleosome eviction first revealed that *gcn5Δ* conferred moderate increases in H3 occupancies in the [–1,NDR,+1] intervals for all ten deciles of genes (Supplementary Figure S13A). Interestingly, however, *gcn5Δ* produced an appreciable reduction in median Rpb1 occupancies (of ∼33%) only for decile D1 (with the highest Rpb3 occupancies), while conferring smaller reductions ranging from 17% to 6% for deciles D2-D7, and little or no reduction for deciles D8-D10 (Figure 6C). Thus, only the most highly expressed constitutive genes are transcriptionally impaired by *gcn5Δ* in the manner shown above for the SM-induced genes. The *eaf1Δ* mutation also produces increased promoter H3 occupancies across deciles 1–10 (Supplementary Figure S13B), to a greater degree than does *gcn5Δ* (Supplementary Figure S13A), in agreement with the heat-map depictions of H3 changes for these mutants shown above (Figure 2A). Moreover, *eaf1Δ* confers larger and broader reductions in median Rpb1 occupancies, ranging from ∼66% to ∼25% for D1 to D10, respectively (Figure 6D), which stands in contrast to the comparable effects of *eaf1Δ* and *gcn5Δ* on Rpb1 occupancies for the SM-induced genes (shown again for comparison in cols. 1–2 of Figure 6C-D).

To explore whether reductions in Rpb1 occupancies conferred by *gcn5Δ* are associated with defects in promoter nucleosome eviction, we sorted the SM-induced genes according to their increases in H3 occupancies in the [-1,NDR,+1] intervals in *gcn5Δ*$_I$ versus WT$_I$ cells (Figure 7A(i) (*top* and *bottom* maps) and plotted the corresponding changes in Rpb1 occupancies for the same gene order (Figure 7A(ii)). The results revealed a tendency for the subsets of both groups of SM-induced genes exhibiting the greatest defects in promoter nucleosome eviction conferred by *gcn5Δ* (at the top of the maps in Figure 7A) to also exhibit larger reductions in Rbp1 occupancies (Figure 7A(ii)). Consistent with these maps, the changes in Rpb1 and H3 occupancies conferred by *gcn5Δ* show a highly significant negative correlation for the 70 SM-induced genes ($\rho = -0.66$, $P < 1 \times 10^{-7}$; Figure 7B). A similar negative correlation was observed between changes in H3 and Rpb1 occupancies conferred by *eaf1Δ* for these genes (Figure 7C, D; $\rho = -0.60$, $P = 1 \times 10^{-7}$). These results are consistent with the idea that defective nucleosome eviction is one contributing factor in the transcriptional reductions conferred by *gcn5Δ* and *eaf1Δ* during induction of the 70 SM-induced genes. Significant, but smaller negative correlations were found for the entire group of 204 genes for both *gcn5Δ* ($\rho = -0.40$, $P = 3 \times 10^{-9}$) and *eaf1Δ* ($\rho = -0.24$, $P = 0.0008$), which might suggest a greater impact on nucleosome repositioning versus eviction, or of recruitment of other co-factors versus nucleosome eviction for the 134 induced genes in the two HAT mutants.

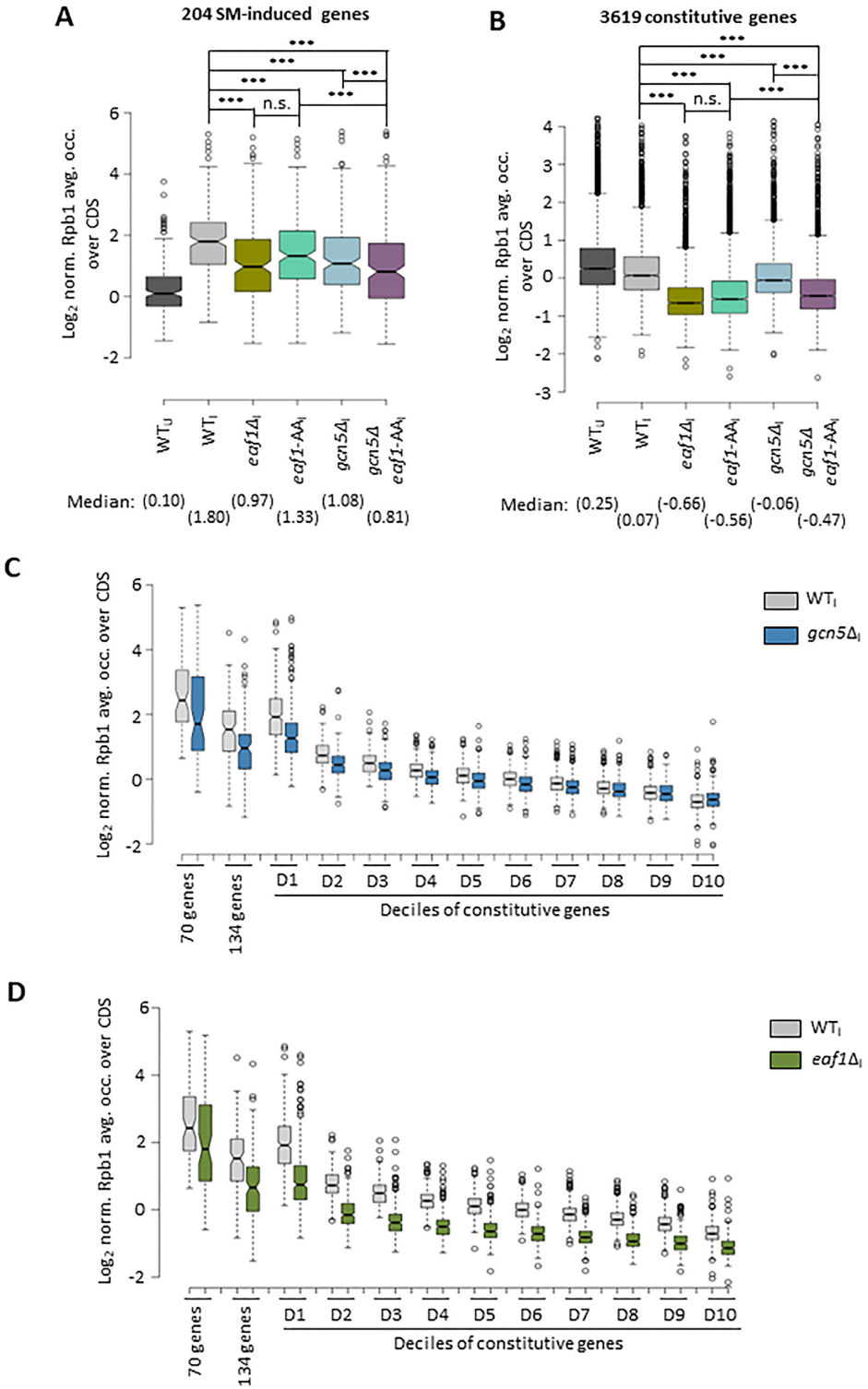

Figure 6. Gcn5 and Eaf1 cooperate in promoting transcription (Pol II occupancies) at both SM-induced genes and highly transcribed constitutive genes. (**A**, **B**) Box plots of $\log_2$ spike-in normalized Rpb1 occupancies per nucleotide in the CDS calculated from ChIP-seq data spike-in normalized using *S. pombe* chromatin for the indicated strains for the 204 SM-induced genes (A) or 3619 constitutive genes (B). (**C**, **D**) $\log_2$ spike-in normalized Rpb1 occupancies across the CDS in WT_I and *gcn5*Δ_I cells (C) or in WT_I and *eaf1*Δ_I cells (D) plotted for the 70 or 134 SM-induced genes (cols. 1 and 2) or for deciles of the 3619 constitutive genes sorted in descending order of their Rpb3 occupancies in WT_I cells. Strains described in Supplementary Figure S8A were employed. Note that here and in subsequent analyses, we have continued to sort genes by transcription rate using our previous relative Rpb3 occupancy data collected from induced WT cells (3) in order to maintain continuity with previous studies on other coactivator mutants and ensure that gene sets being analyzed (e.g. 204 SM-induced or deciles of 3619 constitutively expressed genes) do not vary among our different studies. This approach is justified because spike-in normalization does not change the rank order of genes based on Pol II occupancy for a given strain/condition, so that relative Pol II occupancies yield the same gene order as do spike-in normalized Pol II occupancies.

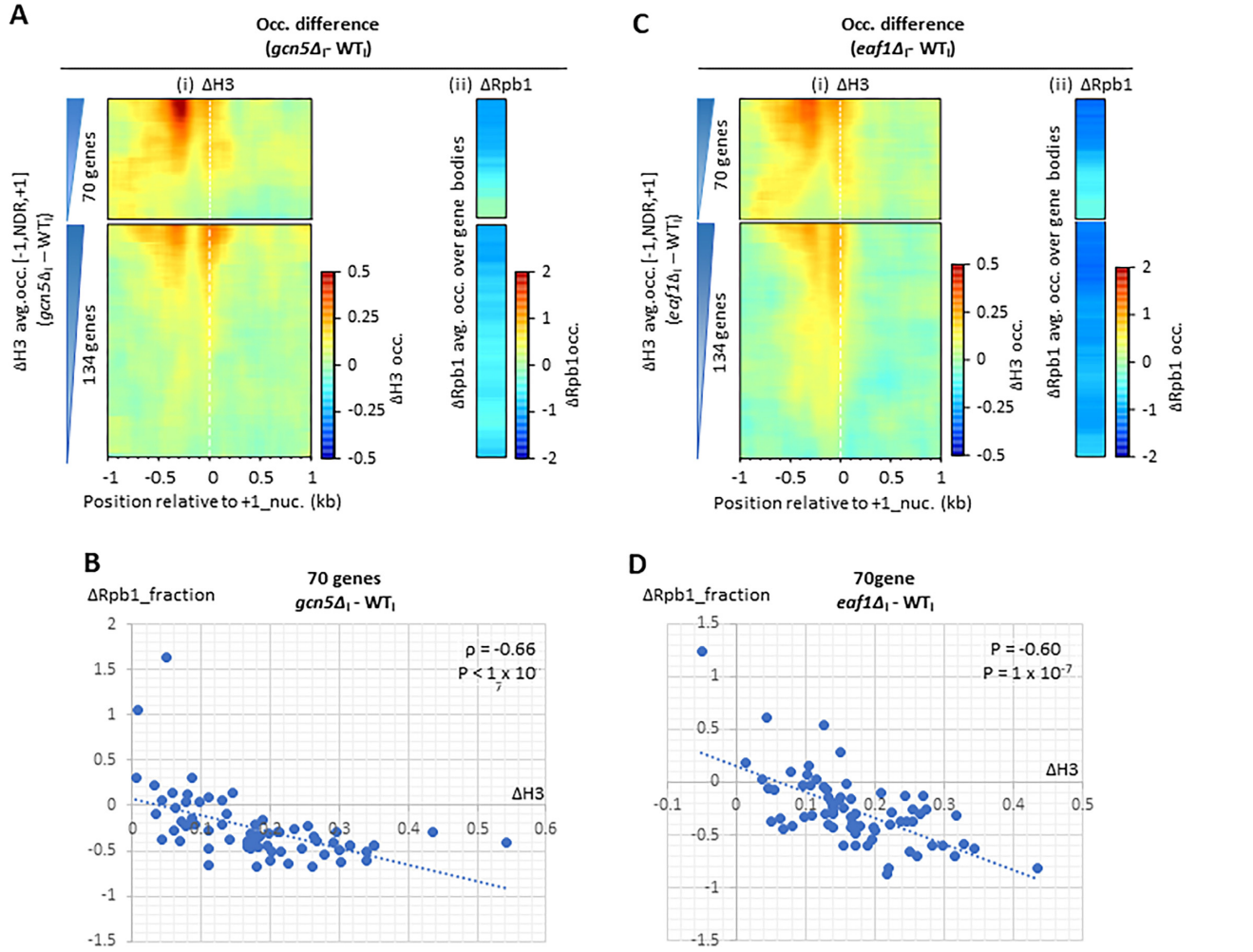

Figure 7. Evidence that defects in promoter nucleosome eviction conferred by *gcn5Δ* and *eaf1Δ* contribute to reduced Pol II occupancies at the 70 SM-induced genes. (**A**) Heat-maps of changes in H3 or Rpb1 occupancies (spike-in normalized) conferred by *gcn5Δ* for the SM-induced genes in induced cells for the 70 and 134 SM-induced genes, each sorted separately according to increases in promoter H3 occupancies between $gcn5\Delta_I$ and WT_I cells from greatest (top) to least (bottom). Differences in occupancies are color-coded as shown by the scale on the right of each panel. (**B**) Scatterplot of fractional changes in spike-in normalized Rpb1 occupancies (Rpb1_$gcn5\Delta_I$ – Rpb1_WT_I)/Rpb1_WT_I) vs. changes in H3 occupancies (H3_$gcn5\Delta_I$ – H3_WT_I) for the 70 SM-induced genes. Spearman coefficient and P-value for the accompanying correlation analysis are indicated. (**C**, **D**) Identical analyses as in (A, B) except for the changes in H3, and Rpb1 occupancies conferred by the *eaf1Δ* mutation. Strains described in Supplementary Figure S8A were employed for all panels.

Diminished Pol II occupancies conferred by *gcn5Δ* are associated with reduced TBP recruitment at SM-induced genes

We asked next whether reductions in Pol II occupancies observed in the HAT mutants might result from diminished promoter occupancies of TATA-binding protein (TBP), a critical component of the PIC. ChIP-seq analysis of native TBP showed a strong SM-induction of TBP occupancies in WT cells, averaged over all 204 induced genes, at the expected location upstream of the TSS (Figure 8A). This induction of TBP binding was confirmed for the individual genes by quantifying the TBP occupancies in the 201 bp intervals surrounding the summits of each TBP peak (Figure 8B); and heat map analysis revealed that induction of TBP occupancies strongly parallels increases in relative Pol II occupancies at the individual genes for the groups of SM-induced genes (Figure 8C (i)-(ii)). Consistent with this, the TBP and Rpb1 occupancies at all 204 induced genes in WT_I cells were highly correlated ($\rho = 0.75$, $P < 1 \times 10^{-7}$), supporting the idea that induced Pol II occupancies reflects increased transcription initiation driven by increased PIC assembly. Importantly, the *gcn5Δ* mutation reduced the average and median TBP occupancies at these genes (Figure 8A, B); and the reductions in TBP and Rpb1 occupancies conferred by *gcn5Δ* were well-correlated for the 204 induced genes ($\rho = 0.59$, $P < 1 \times 10^{-7}$) as expected if defective TBP recruitment contributes to reduced transcription in this HAT mutant. Sorting the SM-induced genes according to their increased promoter H3 occupancies in $gcn5\Delta_I$ versus WT_I cells (as done above in Figure 7A) revealed the largest decreases in TBP occupancies conferred by *gcn5Δ* for the genes at the top of the map exhibiting the greatest defects in H3 eviction for the group of 70 genes (Figure 8D, *top sector*). Consistent with this, the changes in TBP and promoter H3 occupancies produced by *gcn5Δ* show a

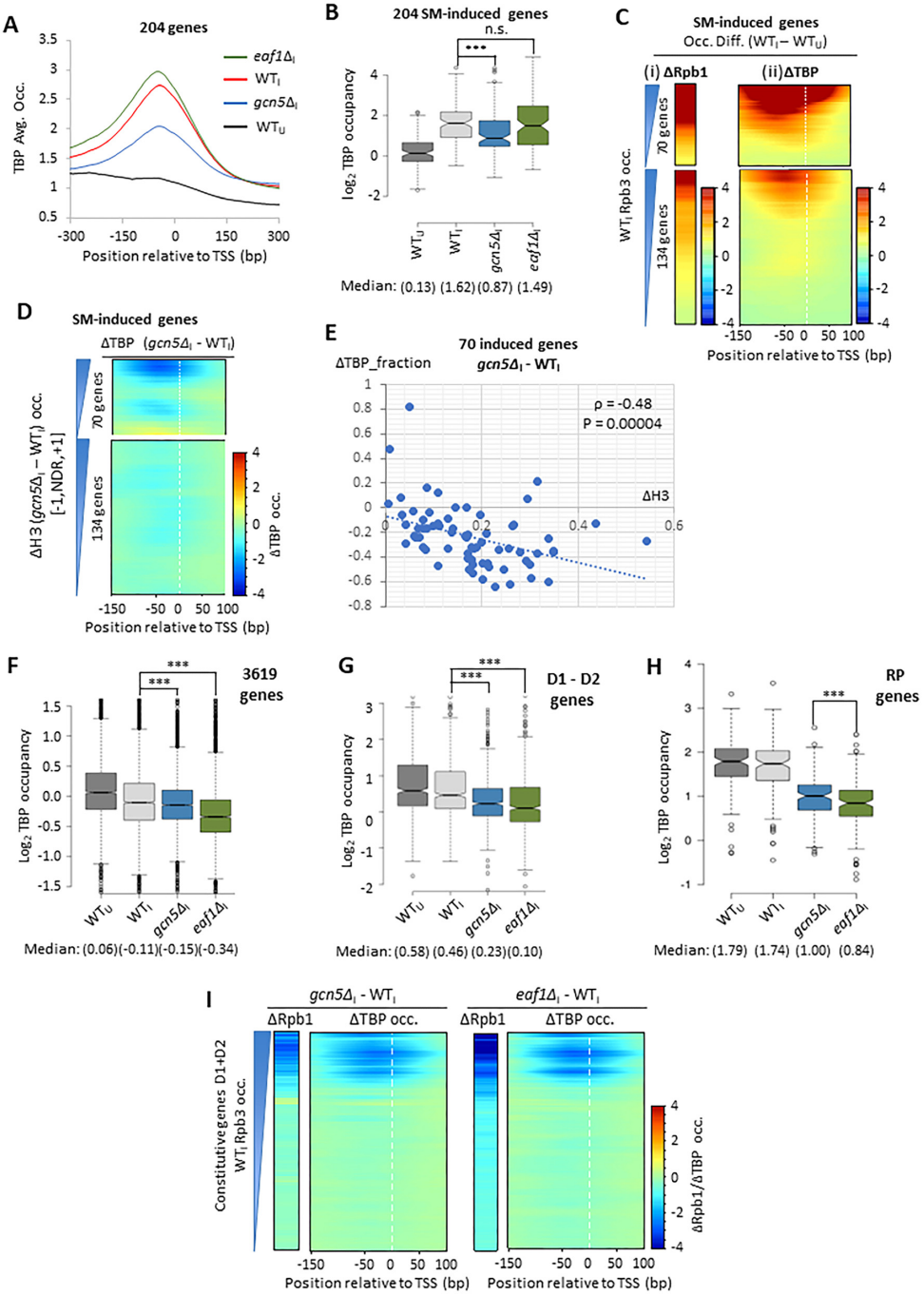

Figure 8. Gcn5 and Eaf1 cooperate in promoting TBP recruitment at SM-induced and highly transcribed constitutive genes. (**A**) Average TBP occupancies calculated from combined TBP ChIP-seq data from three biological replicates plotted relative to the TSS at the 204 SM-induced genes for the indicated strains. (**B**) Box plot of TBP occupancies for the indicated strains calculated from combined ChIP-seq data from three biological replicates for the 116 TBP peaks identified at the 204 SM-induced genes, calculated for the –100 to 100 bp intervals centered on the mode occupancies for each TBP peak. (**C**) Difference maps for induced versus uninduced WT cells for the groups of 70 (*upper*) and 134 (*lower*) SM-induced genes, sorted by their WT_I Rpb3 occupancies for (i) relative Rpb1 occupancies averaged over the CDS or (ii) relative TBP occupancies surrounding the TSS, with the respective occupancy differences color-coded as in the scales to the right of each map. (**D**) TBP occupancy difference maps for $gcn5\Delta_I$ versus WT_I cells for the 70 (*upper*) and 134 (*lower*) SM-induced genes sorted according to their differences in H3 promoter occupancies between $gcn5\Delta_I$ and WT_I cells. (**E**) Scatterplot of fractional changes in TBP occupancies (TBP_$gcn5\Delta_I$ – TBP_WT_I)/TBP_WT_I) versus changes in H3 occupancies (H3_$gcn5\Delta_I$ – H3_WT_I) for the 70 SM-induced genes. Spearman coefficient and *P*-value for the accompanying correlation analysis are indicated. (**F**, **G**) Box plots of TBP occupancies in the [–150 to +100] intervals surrounding the TSSs obtained from combined ChIP-seq data from three biological replicates for all 3619 constitutively expressed genes (F), for only the first two deciles of these genes containing the highest levels of Rpb3 in WT_I cells (G), or for the RP genes (**H**), calculated by averaging the TBP occupancies over the intervals –150 bp to +100 bp surrounding the TSSs of the relevant genes. (**I**) Rpb1 (spike-in normalized) and TBP occupancy difference maps for $gcn5\Delta_I$ versus WT_I cells (*left*) or $eaf1\Delta_I$ versus WT_I cells (*right*) for the constitutive genes in Deciles 1–2 sorted according to their Rpb3 occupancies in WT_I cells. Strains described in Figure 1 were employed for all panels except (**J**), where strains described in Supplementary Figure S8A were used.

significant negative correlation for these genes: $\rho = -0.48$, $P = 4 \times 10^{-5}$ (Figure 8E). (The TBP occupancies at the 134 SM-induced genes are too low to evaluate whether their changes are correlated with H3 increases.) These findings suggest that defective promoter nucleosome eviction contributes to the defects in PIC assembly and transcription conferred by *gcn5Δ* at the most highly induced subset of SM-induced genes. As noted above, defects in nucleosome repositioning or recruitment of other co-factors might also contribute to the diminished TBP recruitment in $gcn5\Delta_I$ versus WT_I cells. Increased promoter H3 occupancies associated with decreased TBP binding to the promoter and diminished Rpb1 in the CDS in $gcn5\Delta_I$ versus WT_I cells is illustrated for two SM-induced genes in Figure 9A, B.

Gcn5 and Eaf1 cooperate in TBP recruitment at highly transcribed constitutively expressed genes

For the two SM-induced genes shown in Figure 9A, B, the *eaf1Δ* mutation resembled *gcn5Δ* in conferring reductions in both TBP and Rpb1 occupancies coupled to increased promoter H3 occupancies. However, *eaf1Δ* did not reduce either the averaged or median TBP occupancy for the entire cohort of 204 SM-induced genes (Figure 8A, B). In contrast, *eaf1Δ* reduces median TBP occupancies for all 3619 constitutive genes, exceeding the small reduction conferred by *gcn5Δ* (Figure 8F), whereas *eaf1Δ* and *gcn5Δ* produce comparable reductions in TBP occupancy at the most highly expressed constitutive genes in deciles D1–D2 (Figure 8G) and at the RP genes (Figure 8H). Moreover, the reductions in TBP recruitment at the D1–D2 genes are strongly associated with reductions in normalized Rpb1 occupancies in both HAT mutants (Figure 8I). Increased promoter H3 occupancies associated with decreased TBP binding and Rpb1 occupancies in the CDS in $gcn5\Delta_I$ and $eaf1\Delta_I$ versus WT_I cells is illustrated for two RP genes and a third constitutively expressed gene (*MFA1*) in Supplementary Figure S14A–C.

The finding that *eaf1Δ* had little effect on TBP recruitment at the SM-induced genes (Figure 8B) while reducing Rpb1 occupancies at these genes *on par* with *gcn5Δ* (Figure 6A) probably results from the fact that we could not normalize the TBP occupancies using the *S. pombe* chromatin spike-in in the manner accomplished for Rpb1 as the TBP antibodies do not immunoprecipitate *S. pombe* TBP. (We attempted to use non-specific immunoprecipitation of *S. pombe* chromatin by these antibodies for normalization but this was unreliable and dramatically increased the variance between biological replicates.) If absolute levels of TBP recruitment are reduced by *eaf1Δ* at the SM-induced genes to a degree similar to the average reduction seen at most other genes, then we would expect to observe no decrease in relative TBP occupancies compared to the average gene. In fact, this result was obtained for Pol II occupancies when we employed Rpb1 or Rpb3 ChIP-seq data that was not spike-in normalized (Supplementary Figure S13C, D). It is likely therefore that *eaf1Δ* reduces absolute TBP occupancies at the SM-induced genes similar in degree to that observed at most other genes, eg. the large group of constitutively expressed genes (Figure 8F). Supporting this interpretation, we observed a strong positive correlation between changes in TBP and Rpb1 occupancies conferred by *eaf1Δ* for all 204 SM-induced genes ($\rho = 0.72$, $P = 0$), in the manner expected if impaired TBP recruitment contributes to reduced transcription in *eaf1Δ* cells. Together, our findings are consistent with the idea that enhancing TBP recruitment is an important aspect of both Gcn5 and NuA4 functions in stimulating transcription initiation, which is executed broadly by NuA4, but restricted to highly expressed constitutive genes and the SM-induced transcriptome for Gcn5.

Gcn5 and NuA4 enhance recruitment of mediator at SM-induced genes

Mediator is a key cofactor involved in recruitment and activation of Pol II (37), and we and others showed previously that Mediator is recruited by Gcn4 and is necessary for robust activation of Gcn4 target genes in SM-starved cells (38–43). Hence, we asked next whether the reductions in transcription conferred by the HAT mutations are associated with defects in Mediator recruitment by conducting ChIP-seq analysis of a myc-tagged version of the Srb6 subunit. Myc-tagging of Srb6 in the WT, *gcn5Δ,* and *eaf1Δ* strains had no detectable effects on cell growth in the presence or absence of SM (Supplementary Figure S15A). In WT cells, Srb6-myc occupancies increased upstream from the TSS and scaled with the induced Rpb3 levels at most of the 70 SM-induced genes, whereas lower levels of Srb6-myc were induced upstream of a subset of the 134 induced genes (Figure 10A(i), (ii)). Interestingly, both *gcn5Δ* and *eaf1Δ* reduced Srb6-myc occupancies under inducing conditions for the majority of the SM-induced genes that exhibit appreciable Srb6-myc occupancies in WT_I cells (Figure 10A(iii)–(iv) versus (ii); Figure 10B). Whereas *gcn5Δ* did not appear to alter expression of Srb6-myc, *eaf1Δ* produced an ∼40% reduction in steady-state Srb6-myc levels (Supplementary Figure S15B), which might contribute to the reduced Srb6-myc occupancies observed in the *eaf1Δ* mutant.

Genes that utilize SAGA or TFIID redundantly and highly transcribed TFIID-dependent genes are similarly hyperdependent on both Gcn5 and NuA4 for promoter nucleosome eviction

Having identified differential requirements for Gcn5 and NuA4 at different genes, we sought to examine the properties of genes exhibiting greater requirements for one of these two HATs in promoter H3 nucleosome eviction. Identifying genes exhibiting a ≥1.4-fold increase in H3 occupancies in the [–1,NDR,+1] intervals in the *gcn5Δ, eaf1Δ,* or *gcn5Δeaf1-AA* mutants compared to WT under inducing conditions, we observed highly significant overlaps among the resulting three groups of genes that appear to be hyperdependent on Gcn5 (Gcn5-Hyp), on Eaf1 (Eaf1-Hyp), or on either one of the two factors (Gcn5/Eaf1-Hyp), for nucleosome eviction (Figure 11A). In particular, ∼75% of the 215 Gcn5-Hyp genes also belong to the group of 405 Eaf1-Hyp genes (Figure 11A), implying that genes with a heightened dependence on one of these HATs tend to similarly require the other for robust promoter nucleosome eviction in WT_I cells. Supporting this idea, the *gcn5Δ* and *eaf1Δ*

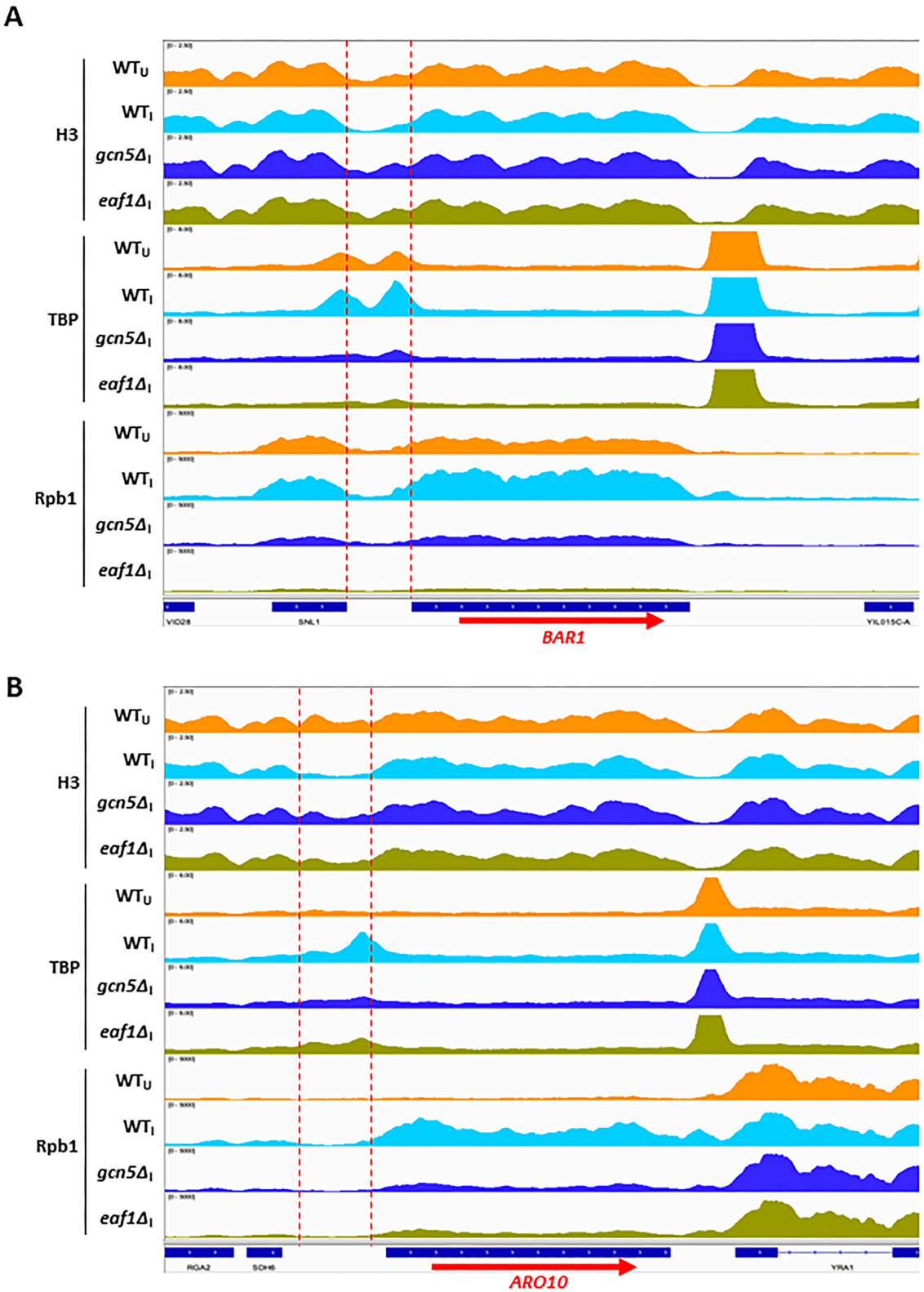

Figure 9. Decreased TBP binding and Pol II occupancies associated with increased promoter H3 occupancies conferred by *gcn5Δ* and *eaf1Δ* at two SM-induced genes. (**A**, **B**) IGV profiles of H3, TBP, and spike-in normalized Rpb1 occupancies from combined ChIP-seq data from three or more biological replicates of WT and mutant strains described in Supplementary Figure S8A for the SM-induced genes *BAR1* (A) and *AR010* (B). Dotted red lines demarcate the [–1,NDR,+1] intervals upstream of the genes.

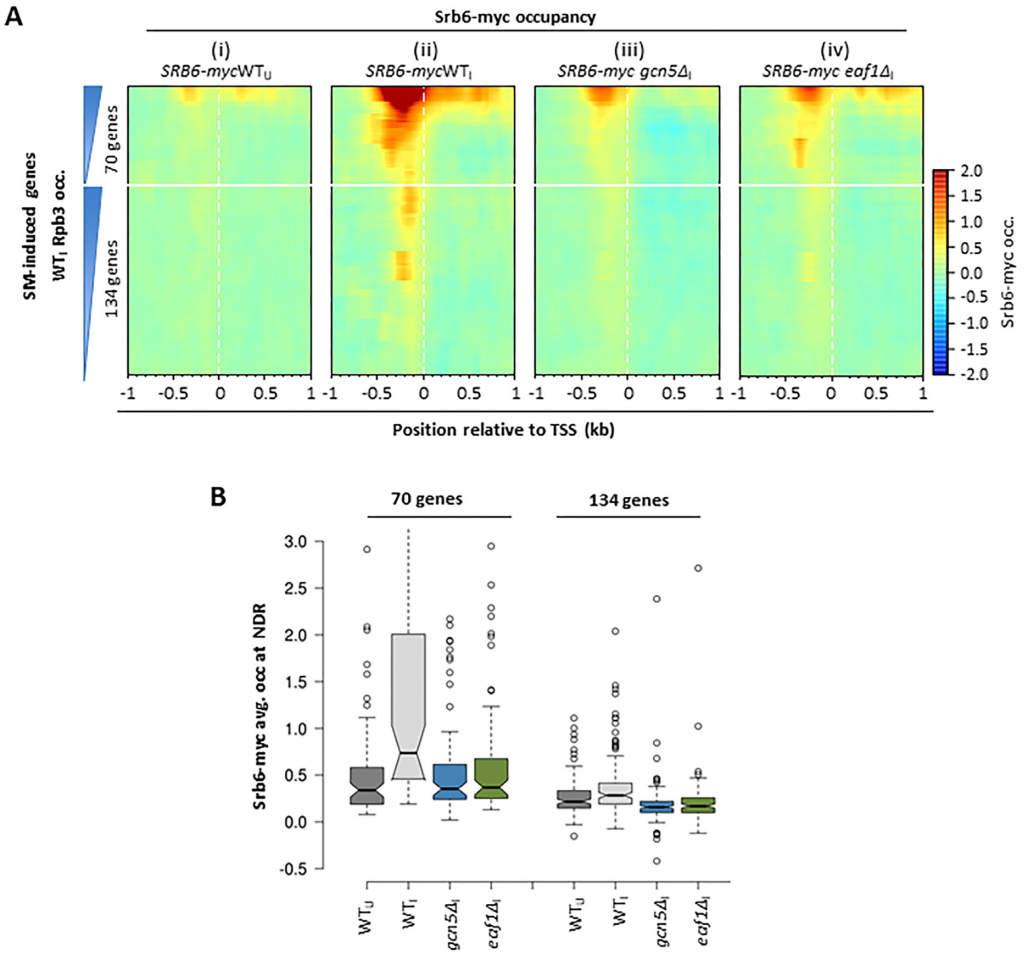

Figure 10. Gcn5 and Eaf1/NuA4 enhance recruitment of Mediator at SM-induced genes. (**A**) WT, *gcn5Δ* or *eaf1Δ* strains harboring *SRB6-myc* (described in Supplementary Figure S15A) and untagged WT strain (BY4741) were cultured in the presence or absence of SM, as in Figure 1, and subjected to ChIP-seq using myc antibodies. Myc occupancies were corrected using the data from the untagged strain cultured under the same conditions. Heat maps of corrected Srb6-myc occupancies are shown for the indicated WT, *gcn5Δ,* or *eaf1Δ* cultures for the 70 (upper) and 134 (lower) sets of SM-induced genes, plotted relative to the TSS and color-coded as shown in the scale to the right of panel (iv). Genes in each group were sorted by their average Rpb3 occupancies over the CDS in WT_I cells (3) as summarized schematically on the left of (i). (**B**) Box plots of $\log_2$corrected Srb6-myc occupancies averaged over the NDR regions for the SM-induced gene groups and the indicated strains/conditions.

mutations both produce marked increases in median H3 promoter occupancies and substantial decreases in Rpb1 occupancies for both the Gcn5-Hyp and Eaf1-Hyp gene sets (Figure 11C-D). Consistent with the functional cooperation between Gcn5 and NuA4 shown above for the SM-induced genes (Figure 3B), these 204 genes are ∼4- to 6-fold enriched for both Gcn5-Hyp and Eaf1-Hyp genes (Supplementary Figure S16A); and 58 of the 70 SM-induced genes are hyper-dependent on Gcn5, Eaf1, or both HATs (Figure 11B; Table 1). As expected from the latter, gene ontology (GO) analysis reveals that Gcn5-Hyp and Eaf1-Hyp groups are enriched for genes involved in amino acid biosynthesis (Table 2). In contrast to the SM-induced genes, the group of 3619 Constitutive genes are slightly depleted for both Gcn5-Hyp and Eaf1-Hyp genes (Supplementary Figure S16B). A different conclusion emerged however if we considered the most highly transcribed subset of the Constitutive genes exhibiting Rpb3 occupancies in WT_I cells greater than one standard deviation above the mean (Z score > 1). This highly expressed (*hex*) subset exhibits significant overlaps for the corresponding *hex* subsets of Gcn5-Hyp and Eaf1-Hyp genes (Supplementary Figure S16C). Thus, both SM-induced and highly-expressed constitutive genes tend to be hyperdependent on both Gcn5 and Eaf1 for promoter nucleosome eviction.

Interestingly, both the Gcn5-Hyp and Eaf1-Hyp genes are enriched for a group of 655 genes previously designated by Hahn *et al.* as being coactivator-redundant (CR) (Supplementary Figure S16D), which exhibit overlapping contributions from SAGA or TFIID for an important function predicted to be TBP recruitment (44). Similar enrichments were observed between a group of 577 genes identified by Pugh *et al.* as being 'SAGA-dominated' (45) (Supplementary Figure S16E), which is expected from the substantial overlap between the CR and SAGA-dominated gene sets ($P = 6 \times 10^{-135}$). Consistent with these results, the 204 SM-induced genes are also highly enriched for both CR ($P = 3 \times 10^{-49}$) and SAGA-dominated genes (3×10^{-31}). Moreover, the *gcn5Δ* and *eaf1Δ* mutations both confer marked increases in median promoter H3 occupancies and

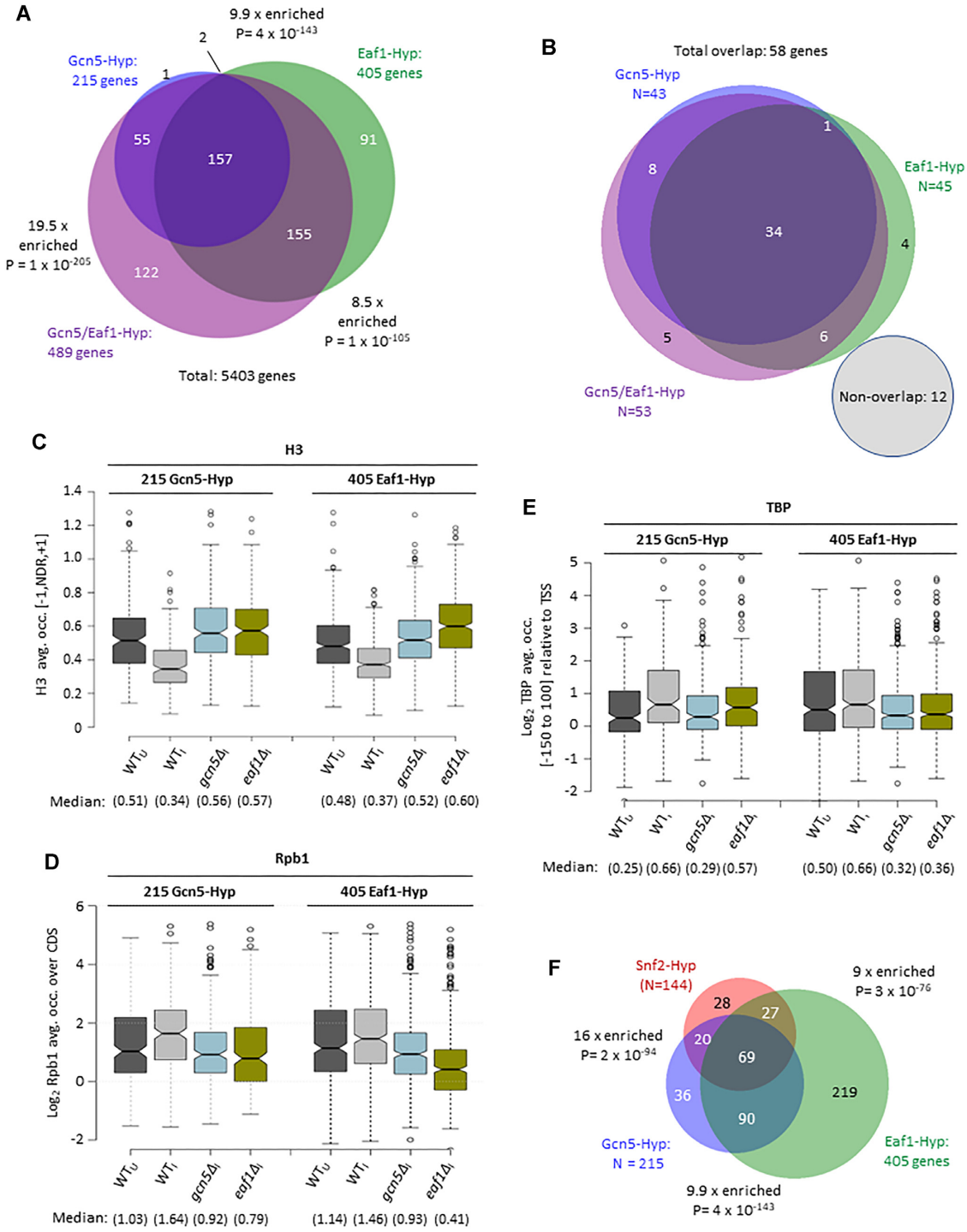

Figure 11. Genes hyperdependent on Gcn5 or Eaf1 for promoter nucleosome eviction frequently require both HATs and chromatin remodelers SWI/SNF for robust eviction in WT cells. (**A**) Venn diagram depicting overlaps of gene sets that are hyperdependent on Gcn5 (blue), Eaf1 (green), or both proteins (magenta) in promoter nucleosome eviction genome-wide. The three sets contain the genes showing >1.4-fold increases in mean H3 occupancies per bp in the [-1,NDR,+1] in *gcn5*Δ_I (Gcn5-Hyp), *eaf1*Δ_I (Eaf1-Hyp), or *gcn5*Δ_I*eaf1-AA*$_I$ (Gcn5/Eaf1-Hyp) mutants versus WT$_I$ cells, determined by H3 ChIP-seq analysis of 3 biological replicates each of the WT or mutant strains engineered for anchor-away under inducing conditions. The degree and significance (P value) of each overlap was assessed using the hypergeometric distribution function and inserted between the labels for the two sets being compared, eg. the Gcn5-Hyp and Eaf1-Hyp groups are 9.9-fold enriched for each other with a *P* value of 4×10^{-143}. (**B**) Venn diagram depicting the distribution of the 70 SM-induced genes among the Gcn5-Hyp, Eaf1-Hyp, and Gcn5/Eaf1-Hyp groups from (A). Only 12 genes, belonging to the fourth (grey) set do not belong to any of the hyperdependent groups. (**C–E**) Box plots of H3 occupancies in the [–1,NDR,+1] intervals (C), $\log_2$ Rpb1 occupancies (spike-in normalized) in the CDS (D), or $\log_2$TBP occupancies in the [–150 to +100] intervals surrounding the TSSs (E) for Gcn5-Hyp or Eaf1-Hyp genes defined as in (A). Strains described in Supplementary Figure S8A were employed for all panels. (**F**) Overlaps between the Gcn5-Hyp and Eaf1-Hyp groups and a similarly defined group of genes hyperdependent on SWI/SNF (Snf2-Hyp) exhibiting > 1.4-fold increases in H3 occupancies averaged over the [–1,NDR,+1] intervals in *snf2*Δ_I vs WT$_I$ cells in our previous study (6).

Table 1. Overlap between the 70 SM-induced genes and genes hyperdependent on Gcn5 or Eaf1 for promoter histone eviction[a]

Overlaps between the 70 SM-induced genes and groups:			
Gcn5-Hyp	Eaf1-Hyp	Gcn5/Eaf1-Hyp	Non-overlapping genes
YBR145W	YBR145W	YBR145W	YBR047W
YBR248C	YBR218C	YBR218C	YDR043C
YBR249C	YBR248C	YBR249C	YDR531W
YCL030C	YBR249C	YCL030C	YGL184C
YDL025C	YCL030C	YCR005C	YIL116W
YDL182W	YCR005C	YDL025C	YIL117C
YDR127W	YDL131W	YDL131W	YJL088W
YDR354W	YDL182W	YDL182W	YJR109C
YDR379C-A	YDR127W	YDL198C	YLL048C
YDR380W	YDR354W	YDR127W	YLR304C
YER052C	YDR379C-A	YDR354W	YOL084W
YER053C	YDR380W	YDR379C-A	YOR303W
YER175C	YER052C	YDR380W	
YFL014W	YER055C	YER052C	
YFL026W	YER069W	YER053C	
YGL032C	YER175C	YER055C	
YGL117W	YFL026W	YER175C	
YGL202W	YGL032C	YFL014W	
YHR018C	YGL117W	YFL026W	
YHR022C	YGL186C	YGL032C	
YIL015W	YGL202W	YGL117W	
YIL051C	YGR161C	YGL186C	
YJR148W	YHR018C	YGL202W	
YKL035W	YHR022C	YGR088W	
YKL211C	YIL015W	YHR018C	
YLL028W	YIL051C	YHR022C	
YLR120C	YJR148W	YHR162W	
YLR258W	YJR154W	YIL015W	
YLR452C	YLL028W	YIL051C	
YMR062C	YLR120C	YJR148W	
YMR251W-A	YLR452C	YKL035W	
YNL036W	YMR062C	YKL211C	
YNL104C	YMR251W-A	YLL028W	
YNL125C	YNL036W	YLR120C	
YNR069C	YNL104C	YLR258W	
YOL052C-A	YNL125C	YLR452C	
YOL119C	YNR069C	YMR062C	
YOR130C	YOL052C-A	YMR251W-A	
YOR230W	YOL058W	YNL036W	
YPL135W	YOR130C	YNL104C	
YPL250C	YOR230W	YNL125C	
YPL264C	YOR337W	YNR044W	
YPR036W-A	YPL135W	YNR069C	
YMR251W-A	YPL250C	YOL052C-A	
YOL052C-A	YPR036W-A	YOL119C	
		YOR130C	
		YOR221C	
		YOR230W	
		YOR337W	
		YPL135W	
		YPL250C	
		YPL264C	
		YPR036W-A	

[a]Data summarized schematically in Figure 11B.

Table 2. GO analysis of genes hyperdependent on Gcn5 or Eaf1 for promoter nucleosome eviction[a]

Category	*P*-value	*k*	*f*
215 Gcn5-Hyp genes, $P < 0.05$, with Bonferroni correction			
Cellular amino acid biosynthetic process [GO:0008652]	1.7×10^{-9}	18	98
Translation [GO:0006412]	1.2×10^{-6}	28	318
Metabolic process [GO:0008152]	2.1×10^{-6}	33	425
405 Eaf1-Hyp genes, $P < 0.05$, with Bonferroni correction			
Translation [GO:0006412]	$<1 \times 10^{-14}$	104	318
Cellular amino acid biosynthetic process [GO:0008652]	2.2×10^{-12}	28	98
Maturation of SSU-rRNA from tricistronic rRNA transcript (SSU-rRNA, 5.8S rRNA, LSU-rRNA) [GO:0000462]	8.8×10^{-9}	18	60
Ribosomal small subunit assembly [GO:0000028]	1.7×10^{-8}	9	14
rRNA export from nucleus [GO:0006407]	1.8×10^{-8}	12	27

[a]Conducted at http://funspec.med.utoronto.ca/cgi-bin/funspec. *k*, number of genes in the GO category present in the Hyp group; *f*, number of genes in the GO category in the genome. *P*-values represent the probability that the intersection of the lists of Hyp genes with the given GO category occurs by chance. The Bonferroni-correction divides the *P*-value threshold, that would be deemed significant for an individual test, by the number of tests conducted and thus accounts for spurious significance due to multiple testing over the categories of a database.

reductions in both Rpb1 and TBP median occupancies at the CR genes; with *eaf1Δ* producing somewhat larger defects than *gcn5Δ* for H3 and Rpb1 (Supplementary Figure S17A–C, CR).

The Gcn5-Hyp and Eaf1-Hyp genes are somewhat depleted (between 1.4-fold and 2-fold) for the much larger group of genes dubbed 'TFIID'-dependent by Hahn *et al.* (44), which rely primarily on TFIID for the function shared between TFIID and SAGA. However, examining the 170 most highly expressed *hex*TFIID-dependent genes reveals strong enrichments for Gcn5-Hyp and Eaf1-Hyp genes, comparable to that seen for the most highly expressed subset of CR genes (Supplementary Figure S16F, G). Hence, the most highly expressed TFIID-dependent genes resemble the CR and SAGA-dominated genes in being strongly dependent on both Gcn5 and Eaf1 for promoter nucleosome eviction.

Whereas *gcn5Δ* and *eaf1Δ* both confer defects in promoter nucleosome eviction at the entire group of TFIID-dependent genes (Supplementary Figure S17A, TFIID-dep); NuA4 is much more important than Gcn5 for TBP recruitment and transcription at these genes (Supplementary Figure S17B, C, TFIID-dep). The findings that Gcn5 and NuA4 function comparably to stimulate transcription of CR genes, whereas NuA4 is more crucial than Gcn5 at the entire group of TFIID-dependent genes, are similar to our conclusions above for the SM-induced versus Constitutive genes (Figure 6C, D). An exception to this generalization emerged from interrogating the 136 genes encoding ribosomal proteins. Although 95% of these RP genes belong to the TFIID-dependent group (44), they are ∼5-fold enriched for the Gcn5-Hyp genes (Figure 12A) and show a much larger reduction of Rpb1 and TBP occupancies in *gcn5Δ* cells (Figure 12C, D) compared to the TFIID-dependent genes on the whole (Supplementary Figure S17B, C, TFIID-dep). They are also highly enriched in Eaf1-Hyp genes (Figure 12A) and strongly dependent on Eaf1 for robust H3 eviction, TBP recruitment and transcription (Figure 12B–D). Thus, the RP genes represent a subset of TFIID-dependent genes exhibiting an atypically strong requirement for both

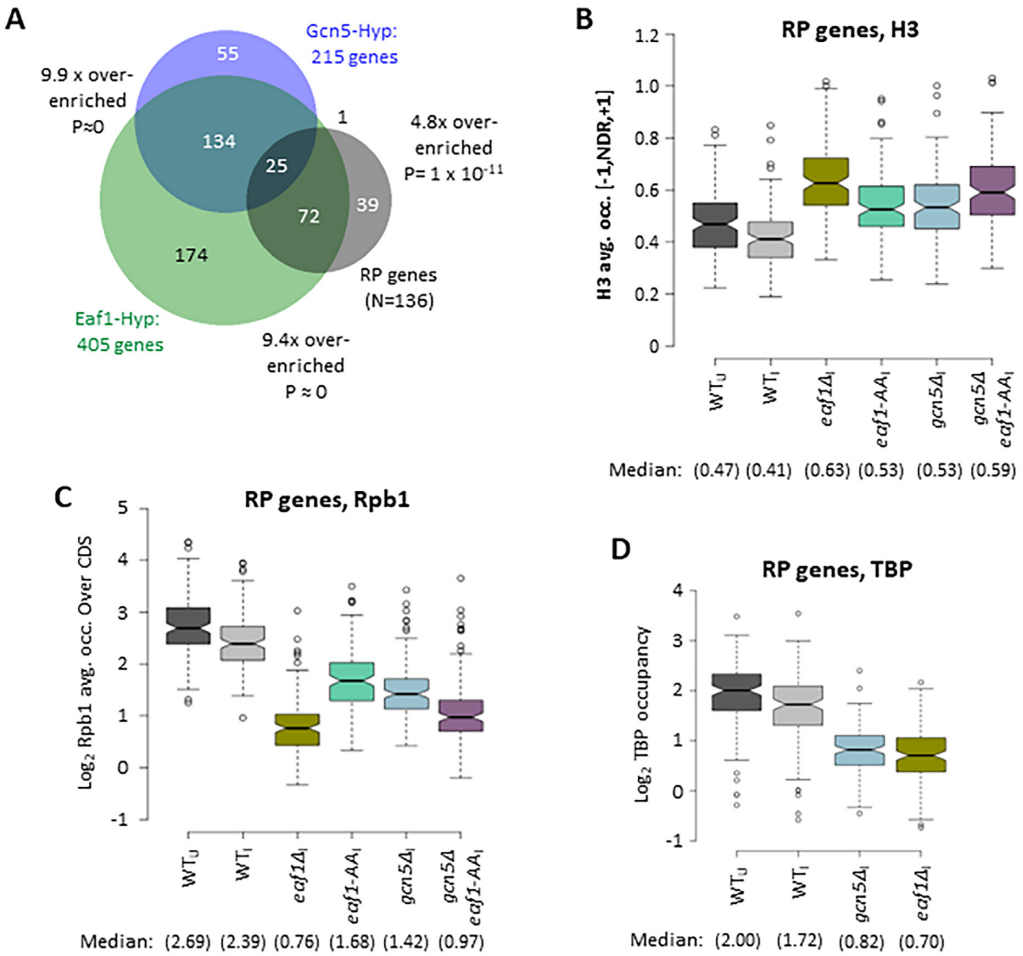

Figure 12. Ribosomal protein genes exhibit strong requirements for both Eaf1/NuA4 and Gcn5 for promoter nucleosome eviction, TBP recruitment and Pol II occupancies. (**A**) Venn diagram depicting the overlaps and enrichments of the Gcn5-Hyp (blue) and Eaf1-Hyp (green) gene sets, defined in Figure 12A, with the 136 ribosomal protein (RP) genes (dark grey). (**B–D**) Box plots of H3 occupancies in the [–1,NDR,+1] intervals (B), $\log_2$ Rpb1 occupancies (spike-in normalized) in CDS (C), or $\log_2$ TBP occupancies in the [-150 to + 100] intervals surrounding the TSSs (D) for the RP genes, for the indicated strains and conditions. Strains described in Supplementary Figure S8A were employed for all panels.

Gcn5 and NuA4 for robust promoter nucleosome eviction, PIC assembly, and transcription. This agrees with the fact that ∼80% of the RP genes are among the most highly-expressed genes in WT_I cells (Rpb3 Z-score > 1) and comprise 60% of the most highly expressed TFIID-dependent genes analyzed in Supplementary Figure S16G.

The results just described indicate that the SM-induced genes, CR genes, and RP genes are enriched for genes hyperdependent on Gcn5 or Eaf1, and they depend almost equally on Gcn5 and Eaf1/NuA4 for WT promoter nucleosome eviction and transcription; whereas the much larger groups of TFIID-dependent genes and 3619 Constitutive genes depend more heavily on Eaf1/NuA4. Consistent with these conclusions, the SM-induced, CR or SAGA-dominated, and most highly expressed subset of the TFIID-dependent genes are enriched for the 5–6% of all genes exhibiting the highest occupancies of SAGA (Spt7-myc) or NuA4 (Eaf1-myc) in their NDR regions (Supplementary Figure S18A–D). Moreover, the latter *hex*TFIID-dependent genes show comparable, high-level median occupancies for both Spt7-myc and Eaf1-myc (Supplementary Figure S18E), whereas the much larger group of weakly expressed TFIID-dependent genes have detectable occupancies only for Eaf1-myc much lower than observed at the *hex*TFIID genes (Supplementary Figure S18E versus F). Thus, the relative occupancies of Spt7-myc versus Eaf1-myc generally correlate with the requirements for SAGA or NuA4 for promoter nucleosome eviction and transcription.

Genes hyperdependent on Gcn5 and NuA4 are similarly dependent on SWI/SNF and RSC for promoter nucleosome eviction

We showed previously that the chromatin remodelers SWI/SNF and RSC display extensive functional cooperation in nucleosome eviction at both SM-induced and highly transcribed constitutively expressed genes (6), which led us to examine here whether genes hyperdependent on the HATs Gcn5 and NuA4 also generally exhibit heightened requirements for these two remodelers. Interrogating our previous H3 ChIP-seq analysis (6) of eliminating Snf2 (by *snf2Δ*) or depleting Sth1 (by transcriptional repres-

sion of P_{TET}-*STH1*)—catalytic subunits of chromatin remodelers SWI/SNF and RSC, respectively—we identified genes hyperdependent on Snf2, Sth1, or either factor showing >1.4-fold increased H3 occupancies in the *snf2*Δ_I, P_{TET}-*STH1*$_I$ or P_{TET}-*STH1snf2*Δ_I mutants versus WT$_I$ cells. Remarkably, there are highly significant overlaps between the three groups of genes hyperdependent on Snf2 or Sth1 and the corresponding Gcn5-Hyp and Eaf1-Hyp groups, which is particularly striking for the Snf2-Hyp group (Figure 11F & Supplementary Figure S19A-B). Furthermore, we found significant positive correlations between increases in promoter H3 occupancies conferred by (i) *snf2*Δ versus *gcn5*Δ, (ii) depletion of Sth1 by P_{TET}-*STH1* versus *eaf1*Δ, and (iii) the P_{TET}-*STH1snf2*Δ and *gcn5*Δ*eaf1-AA* double mutations, for the 70 SM-induced genes (Supplementary Figure S19C–E). All together, our findings suggest that SWI/SNF and RSC frequently cooperate with Gcn5/SAGA and NuA4 in nucleosome eviction at both SM-induced genes and the most highly transcribed constitutive genes in SM-induced WT cells.

DISCUSSION

In this report, we have investigated which of several HATs are most critically required for eviction of promoter nucleosomes and attendant induction of transcription at the group of ∼200 genes induced by amino acid starvation, most of which are activated by transcription factor Gcn4. We employed ChIP-seq analysis of histone H3 to monitor eviction of the H3-H4 tetramer in the nucleosome core from promoter regions, of H3-ac and H4-ac to evaluate acetylation of promoter nucleosomes, and of TBP and Pol II subunits Rpb3 or Rpb1 to assess PIC assembly and transcription. Comparing mutant strains with deletions of the HAT subunits of SAGA (Gcn5), or NuA3 (Sas3), the HAT Rtt109, or two subunits of NuA4 (Eaf1 and Yng2), of which Eaf1 is required for NuA4 integrity, we identified strong requirements for Gcn5 and NuA4, but minor roles for Rtt109 and Sas3, in promoter H3 eviction at the SM-induced genes. Examining the much larger group of 3619 constitutively expressed genes revealed that NuA4 plays a greater role than Gcn5, and that Rtt109 and Sas3 function comparably to Gcn5 in performing ancillary roles in promoter nucleosome eviction at these genes. Overall, we found that NuA4 acts more broadly than the other HATs in promoter nucleosome eviction, but that Gcn5 functions *on par* with NuA4 at the SM-induced genes, the CR group of genes, and the most highly transcribed subset of TFIID-dependent genes that includes most RP genes. Deletion of *GCN5* or *EAF1* broadly reduced H3 and H4 acetylation, respectively, at promoter nucleosomes throughout the genome. Despite strong decreases in H3-ac/H3 and H4-ac/H3 ratios, the degree of reduced acetylation and impaired nucleosome eviction was significantly correlated in both *gcn5*Δ and *eaf1*Δ cells at SM-induced genes, as expected if reduced histone acetylation is an important determinant of impaired nucleosome eviction in these mutants.

We also sought to implicate Gcn5 and Eaf1 in nucleosome eviction following their rapid depletion from the nucleus by AA. The *eaf1-AA* mutation led to elevated H3 occupancies at the various genes affected by *eaf1*Δ, but to a lesser degree compared to the deletion allele, as would be expected from incomplete depletion of Eaf1 from the nucleus. Consistent with this, *eaf1-AA* conferred a smaller reduction than *eaf1*Δ in bulk acetylated H4 as judged by western blot analysis. Despite this limitation, AA of Eaf1 clearly exacerbated the promoter nucleosome eviction defect produced by *gcn5*Δ in the *gcn5*Δ *eaf1-AA* double mutant for all groups of genes tested. This finding indicates that Gcn5 and NuA4 make independent, cumulative contributions to promoter nucleosome eviction throughout the genome. We also attempted to characterize the effects of AA of Gcn5; however, the *gcn5-AA* allele produced little or no reduction in bulk acetylated H3 and could not be pursued further.

Our MNase-ChIP-seq analysis of mutants lacking or depleted of Gcn5 or Eaf1 indicated that these HATs also contribute to the re-positioning of the –1 and +1 promoter nucleosomes, which serves to widen NDRs in WT SM-treated cells by a median value of ∼20 bp. As the TSS frequently lies just inside the upstream boundary of the +1 nucleosome, this repositioning is expected to enhance PIC assembly in the fraction of promoters where eviction of nucleosomes is incomplete. The individual contributions of Gcn5 and NuA4 to the repositioning are modest, although the degree of NDR narrowing observed in the *eaf1-AA gcn5*Δ double mutant is comparable to that we reported previously for cells lacking SWI/SNF function (6). In that report we also showed evidence that SWI/SNF and the essential remodeler RSC have additive functions in both repositioning and evicting promoter nucleosomes, as a double mutant impaired for both remodelers exhibited greater defects versus the single mutants. Here we found that genes with a heightened dependence on Gcn5 or Eaf1 for promoter nucleosome eviction, which overlap extensively and include both SM-induced and highly transcribed constitutively expressed genes, tend to be similarly hyperdependent on SWI/SNF and RSC. Moreover, the degree of increased nucleosome occupancies conferred by *gcn5*Δ and *eaf1*Δ are correlated with those given by eliminating or depleting the catalytic subunits of these remodelers at SM-induced genes. Thus, it appears that multiple remodelers and HATs functionally collaborate in both repositioning and evicting the -1 and + 1 nucleosomes at both SM-induced and highly expressed constitutive genes. We further showed here that both SAGA (Spt7-myc) and NuA4 (Eaf1-myc) are recruited to many SM-induced and highly transcribed constitutive genes, as demonstrated previously for SWI/SNF and RSC (6), providing evidence that these multiple cofactors all function directly to enhance promoter nucleosome remodeling. Whether they act simultaneously or sequentially at the same promoters remains an open question.

In accordance with the contributions of Gcn5 and Eaf1/NuA4 to ejecting promoter nucleosomes at SM-induced genes, eliminating each HAT reduced Pol II occupancies at these genes, as judged by spike-in normalized Rpb1 ChIP-seq. Moreover, these reductions showed a significant inverse correlation with defects in H3 eviction in both *gcn5*Δ and *eaf1*Δ cells. *gcn5*Δ also conferred reduced TBP occupancies in the promoter regions of SM-induced genes, similar in magnitude to the reductions in Pol II occupancies. These findings are consistent with the idea that

eliminating Gcn5 or NuA4 impairs promoter nucleosome eviction with attendant reduced PIC assembly and diminished transcription initiation at SM-induced genes. It seems likely that impaired nucleosome sliding (versus eviction) and reduced recruitment of one or more other cofactors by acetylated H3/H4 tails also contribute to the diminished transcription of these genes in both HAT mutants.

In agreement with conferring relatively stronger defects in histone eviction at the 3619 constitutively expressed genes, *eaf1Δ* produced a greater reduction in Rpb1 occupancies compared to *gcn5Δ* for this large gene cohort. The *eaf1Δ* mutation also conferred a broader reduction in TBP occupancies compared to *gcn5Δ* at the constitutively expressed genes. However, Gcn5 functions *on par* with Eaf1/NuA4 in both TBP recruitment and transcription at the most highly transcribed subset of constitutive genes, including the RP genes, just as we observed at SM-induced genes. The relative importance of Gcn5 and NuA4 for TBP recruitment and transcription generally scales with their contributions to promoter nucleosome eviction at the respective genes, providing additional evidence that nucleosome ejection is an important aspect of their stimulatory effects on PIC assembly and transcription. Note that we cannot eliminate the possibility that reductions in PIC assembly or transcription conferred by impairing Gcn5 and NuA4, which do not involve diminished nucleosome acetylation or eviction, could lead indirectly to increased nucleosome occupancies in promoters.

As mentioned, the genes with heightened dependence on Gcn5 or Eaf1/NuA4 for promoter nucleosome eviction (the Gcn5-hyp and Eaf1-hyp groups) are also generally hyperdependent on the other HAT for WT levels of nucleosome eviction. This functional overlap is prominent for the SM-induced genes, the CR group of genes that utilize both SAGA and TFIID as cofactors, and the subset of the most highly transcribed TFIID-dependent genes, which includes most RP genes. It was possible that Gcn5 and NuA4 would have completely redundant functions, such that eliminating only one HAT in each single mutant would have no impact on nucleosome eviction. While we identified 122 genes as being Eaf1/Gcn5-hyperdependent only in the *eaf1-AA gcn5Δ* double (Figure 11A), most of these genes still showed increased nucleosome occupancies in each single mutant, and merely display greater defects in the double mutant, indicating non-redundant contributions of Gcn5 and NuA4 to nucleosome eviction. The same is true for the TFIID-dependent genes that exhibit a significant contribution from Gcn5 that is simply smaller than that attributable to NuA4. One way to explain the non-redundant functions of these two HATs is to propose that H3 acetylation by Gcn5 and H4 acetylation by NuA4 make independent, additive contributions to nucleosome eviction or sliding, either by reducing chromatin compaction or stimulating the recruitment via acetylated histones of other co-factors involved in nucleosome remodeling.

Interestingly, we found that *gcn5Δ* has a greater effect on TBP recruitment and transcription at the CR versus TFIID genes (Supplementary Figure S17C), supporting the proposal that SAGA functionally cooperates with TFIID in TBP recruitment primarily at CR genes (44). In contrast, *eaf1Δ* reduces TBP recruitment more equally at both CR and TFIID genes (Supplementary Figure S17C). Huisinga and Pugh also divided most yeast genes into two groups depending on whether their transcription was strongly impaired by inactivation of TFIID subunit Taf1 ('TFIID-dominated') or by inactivation of Taf1 only in cells also lacking SAGA subunit Spt3 and moderately impaired by elimination of Spt3 alone ('SAGA-dominated' genes). In fact, the functionally related CR and SAGA-dominated gene sets overlap extensively, and each is enriched for both Gcn5- and Eaf1-hyperdependent genes (Supplementary Figure S16D, E) and for the ∼6% of genes with the highest occupancies of SAGA (Spt7-myc) and NuA4 (Eaf1-myc) in WT_I cells (Supplementary Figure S18C, D). Interestingly, the 170 TFIID-dependent genes of Donczew et al. (2020) most highly transcribed in WT_I cells (*hex*TFIID), of which 60% are RP genes, are equally likely as CR/SAGA-dominated genes to recruit SAGA and NuA4 (Supplementary Figure S18B versus C–D; Supplementary Figure S18E) and to be hyperdependent on Gcn5/SAGA and Eaf1/NuA4 for nucleosome eviction (Supplementary Figure S16G versus D–F). Our finding that Gcn5 contributes substantially to histone eviction and transcription of certain TFIID-dependent genes, including RP genes, is consistent with previous findings on the effects of deleting subunits required for SAGA integrity, and was attributed to a requirement at both CR and TFIID genes for the histone modification functions of SAGA in addition to SAGA's role in recruiting TBP (44). It is also consistent with previous observations by Huisinga and Pugh that Gcn5 enhances transcription of both SAGA-dominated and TFIID-dominated genes (45). The vast majority of TFIID-dependent genes show a greater dependence on Eaf1 versus Gcn5 for histone eviction and transcription (Supplementary Figure S17A–C) and also selectively bind NuA4, albeit at low levels (Supplementary Figure S18F).

Bruzzone *et al.* reported that AA of either Gcn5 or the NuA4 catalytic subunit Esa1 led to genome-wide reductions in acetylated H4 or acetylated H3 in promoter regions and reduced transcription of the affected genes, but which was not accompanied by significant changes in H3 occupancies or nucleosome positions (16). It seems possible that their AA of Gcn5 or Esa1 did not reduce the HAT functions sufficiently to produce the defects in nucleosome eviction we observed in *gcn5Δ* and *eaf1Δ* strains. Indeed, we and others observed that AA of various cofactors confers weaker mutant phenotypes compared to the corresponding deletion mutations (34) (12). Consistent with this explanation, we found that AA of Eaf1 conferred increased H3 occupancies that were merely less extensive than that given by *eaf1Δ*. We could not provide similar evidence for Gcn5 because AA of Gcn5 in our strain had only minimal effects on H3 acetylation; thus, we cannot dismiss the possibility that the defects in nucleosome eviction we observed in *gcn5Δ* cells require a chronic loss of Gcn5 HAT activity that leads indirectly to altered expression of other factors involved in transcription. One argument against this scenario is that SAGA, as well as NuA4, is directly recruited to the SM-induced genes on Gcn4 induction. Nevertheless, the findings of reduced transcription without detectable defects in nucleosome remodeling of Bruzzone et al. suggest that Gcn5 and NuA4 can stimulate transcription at least partly by enhancing

recruitment of other cofactors via acetylated histones, or by acetylating the cofactors themselves.

Bruzzone et al. reported that AA of Esa1 or Gcn5 conferred reductions in Rpb1 occupancies that were more widespread and extensive for Esa1 compared to Gcn5, which is similar to our conclusions reached from *gcn5Δ* and *eaf1Δ* mutants. We further provided evidence that TBP recruitment is impaired at genes where transcription is diminished in *eaf1Δ* and *gcn5Δ* mutants. In cells treated with diamide, where ∼1400 genes were induced, these workers observed little effect of Gcn5 depletion, whereas Esa1 depletion broadly dampened gene induction. For the SM-induced transcriptome, by contrast, our results suggest that Gcn5 and NuA4 both make important contributions to transcriptional induction. We came to the same conclusion for the most highly transcribed subset of constitutively expressed genes, particularly the RP genes that are so crucial for robust cell growth.

In conclusion, our findings indicate that Gcn5 and NuA4 functionally cooperate to enhance the repositioning and eviction of promoter nucleosomes in a manner that stimulates PIC assembly and attendant transcription of the majority of highly expressed genes, to which they are recruited. These genes include those induced by Gcn4 in amino acid-starved cells, which generally require SAGA for promoter activation, and also the most highly transcribed and TFIID-dependent constitutively expressed genes, including those encoding ribosomal proteins.

DATA AVAILABILITY

All raw and processed sequencing data generated in this study have been submitted to the NCBI Gene Expression Omnibus (GEO; http://www.ncbi.nlm.nih.gov/geo/) under accession number GSE207278. The processed ChIP-seq data averaged over all biological replicates are provided for all expressed genes, and for specific genes sets analyzed in each figure, in supplementary File S1 to File S9, File S11 and File S12, and the gene lists are given in supplementary File S10.

SUPPLEMENTARY DATA

Supplementary Data are available at NAR Online.

ACKNOWLEDGEMENTS

We thank Joe Reese for TBP antibodies, and all members of our groups and those of Tom Dever, Nick Guydosh and Jon Lorsch for their many helpful suggestions.

FUNDING

Intramural Research Program of the NIH (in part); NIH HPC Biowulf cluster (http://hpc.nih.gov); NHLBI DNA Sequencing and Genomics Core facility. Funding for open access charge: Intramural Program of the National Institutes of Health.
Conflict of interest statement. None declared.

REFERENCES

1. Boeger,H., Griesenbeck,J., Strattan,J.S. and Kornberg,R.D. (2003) Nucleosomes unfold completely at a transcriptionally active promoter. *Mol. Cell*, **11**, 1587–1598.
2. Reinke,H. and Horz,W. (2003) Histones are first hyperacetylated and then lose contact with the activated PHO5 promoter. *Mol. Cell*, **11**, 1599–1607.
3. Qiu,H., Chereji,R.V., Hu,C., Cole,H.A., Rawal,Y., Clark,D.J. and Hinnebusch,A.G. (2016) Genome-wide cooperation by HAT Gcn5, remodeler SWI/SNF, and chaperone Ydj1 in promoter nucleosome eviction and transcriptional activation. *Genome Res.*, **26**, 211–225.
4. Reja,R., Vinayachandran,V., Ghosh,S. and Pugh,B.F. (2015) Molecular mechanisms of ribosomal protein gene coregulation. *Genes Dev.*, **29**, 1942–1954.
5. Nocetti,N. and Whitehouse,I. (2016) Nucleosome repositioning underlies dynamic gene expression. *Genes Dev.*, **30**, 660–672.
6. Rawal,Y., Chereji,R.V., Qiu,H., Ananthakrishnan,S., Govind,C.K., Clark,D.J. and Hinnebusch,A.G. (2018) SWI/SNF and RSC cooperate to reposition and evict promoter nucleosomes at highly expressed genes in yeast. *Genes Dev.*, **32**, 695–710.
7. Parnell,T.J., Huff,J.T. and Cairns,B.R. (2008) RSC regulates nucleosome positioning at Pol II genes and density at Pol III genes. *EMBO J.*, **27**, 100–110.
8. Badis,G., Chan,E.T., van Bakel,H., Pena-Castillo,L., Tillo,D., Tsui,K., Carlson,C.D., Gossett,A.J., Hasinoff,M.J., Warren,C.L. *et al.* (2008) A library of yeast transcription factor motifs reveals a widespread function for Rsc3 in targeting nucleosome exclusion at promoters. *Mol. Cell*, **32**, 878–887.
9. Hartley,P.D. and Madhani,H.D. (2009) Mechanisms that specify promoter nucleosome location and identity. *Cell*, **137**, 445–458.
10. Ganguli,D., Chereji,R.V., Iben,J.R., Cole,H.A. and Clark,D.J. (2014) RSC-dependent constructive and destructive interference between opposing arrays of phased nucleosomes in yeast. *Genome Res.*, **24**, 1637–1649.
11. Parnell,T.J., Schlichter,A., Wilson,B.G. and Cairns,B.R. (2015) The chromatin remodelers RSC and ISW1 display functional and chromatin-based promoter antagonism. *Elife*, **4**, e06073.
12. Qiu,H., Biernat,E., Govind,C.K., Rawal,Y., Chereji,R.V., Clark,D.J. and Hinnebusch,A.G. (2020) Chromatin remodeler Ino80C acts independently of H2A.Z to evict promoter nucleosomes and stimulate transcription of highly expressed genes in yeast. *Nucleic Acids Res.*, **48**, 8408–8430.
13. Sterner,D.E. and Berger,S.L. (2000) Acetylation of histones and transcription-related factors. *Microbiol. Mol. Biol. Rev.*, **64**, 435–459.
14. Ginsburg,D.S., Govind,C.K. and Hinnebusch,A.G. (2009) The NuA4 lysine acetyltransferase Esa1 is targeted to coding regions and stimulates transcription elongation with Gcn5. *Mol. Cell. Biol.*, **29**, 6473–6487.
15. Brown,C., Howe,L., Sousa,K., Alley,S.C., Carrozza,M.J., Tan,S. and Workman,J.L. (2001) Recruitment of HAT complexes by direct activator interactions with the AATM-related tra1 subunit. *Science*, **292**, 2333.
16. Bruzzone,M.J., Grunberg,S., Kubik,S., Zentner,G.E. and Shore,D. (2018) Distinct patterns of histone acetyltransferase and Mediator deployment at yeast protein-coding genes. *Genes Dev.*, **32**, 1252–1265.
17. Winzeler,E.A., Shoemaker,D.D., Astromoff,A., Liang,H., Anderson,K., Andre,B., Bangham,R., Benito,R., Boeke,J.D., Bussey,H. *et al.* (1999) Functional characterization of the *S. cerevisiae* genome by gene deletion and parallel analysis. *Science*, **285**, 901–906.
18. Longtine,M.S., McKenzie,A. III, Demarini,D.J., Shah,N.G., Wach,A., Brachat,A., Philippsen,P. and Pringle,J.R. (1998) Additonal modules for versatile and economical PCR-based gene deletion and modification in *Saccharomyces cerevisiae*. *Yeast*, **14**, 953–961.
19. Goldstein,A.L. and McCusker,J.H. (1999) Three new dominant drug resistance cassettes for gene disruption in Saccharomyces cerevisiae. *Yeast*, **15**, 1541–1553.
20. Qiu,H., Hu,C., Gaur,N.A. and Hinnebusch,A.G. (2012) Pol II CTD kinases Bur1 and Kin28 promote Spt5 CTR-independent recruitment of Paf1 complex. *EMBO J.*, **31**, 3494–3505.
21. Cole,H.A., Ocampo,J., Iben,J.R., Chereji,R.V. and Clark,D.J. (2014) Heavy transcription of yeast genes correlates with differential loss of histone H2B relative to H4 and queued RNA polymerases. *Nucleic Acids Res.*, **42**, 12512–12522.

22. Zhang,F., Gaur,N.A., Hasek,J., Kim,S.J., Qiu,H., Swanson,M.J. and Hinnebusch,A.G. (2008) Disrupting vesicular trafficking at the endosome attenuates transcriptional activation by Gcn4. *Mol. Cell. Biol.*, **28**, 6796–6818.
23. Langmead,B. and Salzberg,S.L. (2012) Fast gapped-read alignment with Bowtie 2. *Nat. Methods*, **9**, 357–359.
24. Robinson,J.T., Thorvaldsdottir,H., Winckler,W., Guttman,M., Lander,E.S., Getz,G. and Mesirov,J.P. (2011) Integrative genomics viewer. *Nat. Biotechnol.*, **29**, 24–26.
25. Rawal,Y., Chereji,R.V., Valabhoju,V., Qiu,H., Ocampo,J., Clark,D.J. and Hinnebusch,A.G. (2018) Gcn4 binding in coding regions can activate internal and canonical 5' promoters in yeast. *Mol. Cell*, **70**, 297–311.
26. Mitchell,L., Lambert,J.P., Gerdes,M., Al-Madhoun,A.S., Skerjanc,I.S., Figeys,D. and Baetz,K. (2008) Functional dissection of the NuA4 histone acetyltransferase reveals its role as a genetic hub and that Eaf1 is essential for complex integrity. *Mol. Cell. Biol.*, **28**, 2244–2256.
27. Auger,A., Galarneau,L., Altaf,M., Nourani,A., Doyon,Y., Utley,R.T., Cronier,D., Allard,S. and Cote,J. (2008) Eaf1 is the platform for NuA4 molecular assembly that evolutionarily links chromatin acetylation to ATP-dependent exchange of histone H2A variants. *Mol. Cell. Biol.*, **28**, 2257–2270.
28. Searle,N.E., Torres-Machorro,A.L. and Pillus,L. (2017) Chromatin regulation by the NuA4 acetyltransferase complex is mediated by essential interactions between enhancer of polycomb (Epl1) and Esa1. *Genetics*, **205**, 1125–1137.
29. Brachmann,C.B., Davies,A., Cost,G.J., Caputo,E., Li,J., Hieter,P. and Boeke,J.D. (1998) Designer deletion strains derived from Saccharomyces cerevisiae S288C: a useful set of strains and plasmids for PCR-mediated gene disruption and other applications. *Yeast*, **14**, 115–132.
30. D'Arcy,S. and Luger,K. (2011) Understanding histone acetyltransferase Rtt109 structure and function: how many chaperones does it take?*Curr. Opin. Struct. Biol.*, **21**, 728–734.
31. John,S., Howe,L., Tafrov,S.T., Grant,P.A., Sternglanz,R. and Workman,J.L. (2000) The something about silencing protein, Sas3, is the catalytic subunit of NuA3, a yTAF(II)30-containing HAT complex that interacts with the Spt16 subunit of the yeast CP (Cdc68/Pob3)-FACT complex. *Genes Dev.*, **14**, 1196–1208.
32. Babiarz,J.E., Halley,J.E. and Rine,J. (2006) Telomeric heterochromatin boundaries require NuA4-dependent acetylation of histone variant H2A.Z in Saccharomyces cerevisiae. *Genes Dev.*, **20**, 700–710.
33. Haruki,H., Nishikawa,J. and Laemmli,U.K. (2008) The anchor-away technique: rapid, conditional establishment of yeast mutant phenotypes. *Mol. Cell*, **31**, 925–932.
34. Petrenko,N., Jin,Y., Wong,K.H. and Struhl,K. (2017) Evidence that Mediator is essential for Pol II transcription, but is not a required component of the preinitiation complex in vivo. *Elife*, **6**, e28447.
35. Ocampo,J., Chereji,R.V., Eriksson,P.R. and Clark,D.J. (2016) The ISW1 and CHD1 ATP-dependent chromatin remodelers compete to set nucleosome spacing in vivo. *Nucleic Acids Res.*, **44**, 4625–4635.
36. Zhang,L., Ma,H. and Pugh,B.F. (2011) Stable and dynamic nucleosome states during a meiotic developmental process. *Genome Res.*, **21**, 875–884.
37. Hahn,S. and Young,E.T. (2011) Transcriptional regulation in Saccharomyces cerevisiae: transcription factor regulation and function, mechanisms of initiation, and roles of activators and coactivators. *Genetics*, **189**, 705–736.
38. Natarajan,K., Jackson,B.M., Zhou,H., Winston,F. and Hinnebusch,A.G. (1999) Transcriptional activation by Gcn4p involves independent interactions with the SWI/SNF complex and SRB/mediator. *Mol.Cell*, **4**, 657–664.
39. Swanson,M.J., Qiu,H., Sumibcay,L., Krueger,A., Kim,S.-J., Natarajan,K., Yoon,S. and Hinnebusch,A.G. (2003) A multiplicity of coactivators is required by Gcn4p at individual promoters in vivo. *Mol.Cell.Biol*, **23**, 2800–2820.
40. Qiu,H., Hu,C., Yoon,S., Natarajan,K., Swanson,M.J. and Hinnebusch,A.G. (2004) An array of coactivators is required for optimal recruitment of TATA binding protein and RNA polymerase II by promoter-bound Gcn4p. *Mol. Cell. Biol.*, **24**, 4104–4117.
41. Zhang,F., Sumibcay,L., Hinnebusch,A.G. and Swanson,M.J. (2004) A triad of subunits from the Gal11/tail domain of Srb mediator is an in vivo target of transcriptional activator Gcn4p. *Mol. Cell. Biol.*, **24**, 6871–6886.
42. Jedidi,I., Zhang,F., Qiu,H., Stahl,S.J., Palmer,I., Kaufman,J.D., Nadaud,P.S., Mukherjee,S., Wingfield,P.T., Jaroniec,C.P. *et al.* (2010) Activator Gcn4 employs multiple segments of Med15/Gal11, including the KIX domain, to recruit mediator to target genes in vivo. *J. Biol. Chem.*, **285**, 2438–2455.
43. Brzovic,P.S., Heikaus,C.C., Kisselev,L., Vernon,R., Herbig,E., Pacheco,D., Warfield,L., Littlefield,P., Baker,D., Klevit,R.E. *et al.* (2011) The acidic transcription activator Gcn4 binds the mediator subunit Gal11/Med15 using a simple protein interface forming a fuzzy complex. *Mol. Cell*, **44**, 942–953.
44. Donczew,R., Warfield,L., Pacheco,D., Erijman,A. and Hahn,S. (2020) Two roles for the yeast transcription coactivator SAGA and a set of genes redundantly regulated by TFIID and SAGA. *Elife*, **9**, e50109.
45. Huisinga,K.L. and Pugh,B.F. (2004) A genome-wide housekeeping role for TFIID and a highly regulated stress-related role for SAGA in Saccharomyces cerevisiae. *Mol. Cell*, **13**, 573–585.